Incorporating Structure-from-Motion (SfM) Photogrammetry into Sedimentation Monitoring

Incorporating Structure-from-Motion (SfM) Photogrammetry into Sedimentation Monitoring

Final Report

Prepared By:

Rolando O. Santos[1]

Nicolas Rivas[1]

Xaymara Serrano[2]

[1]Institute of the Environment

Florida International University, Miami, FL 33189

[2]NOAA National Marine Fisheries Service

Southeast Regional Office, Habitat Conservation Division

West Palm Beach, FL, 33401

June 2026

Completed in Fulfillment of C6A83A for

Florida Department of Environmental Protection
Coral Protection and Restoration Program
8000 N Ocean Dr.
Dania Beach, FL 33004

This final report should be cited as follows:
Santos RO, Rivas N, Serrano X. 2026. Incorporating structure-from-motion photogrammetry into sedimentation monitoring. Final Report. Florida DEP. 1-44.

This report was funded through a contract agreement from the Florida Department of Environmental Protection's (DEP) Coral Protection and Restoration Program. The views, statements, findings, conclusions, and recommendations expressed herein are those of the author(s) and do not necessarily reflect the views of the State of Florida or any of its subagencies.

ACKNOWLEDGEMENTS

We thank the Florida Department of Environmental Protection for their support of this project, particularly Elena Kampian and Yesmarie DeLaFlor for their guidance and collaboration throughout the study. We are also grateful to members of the Santos Seascape Ecology Lab, especially Hannah-Marie Lamle, Valentina Bautista, Gina Badlowski, and Marianna Coppola, for their invaluable assistance with fieldwork, data collection, and processing. Additional thanks are extended to volunteers Mariella Torres, Emily Jackson, and Brandon Sosa for their support in the field and to Florida International University's Oceans and Coastlines division for their support. This material is also based upon work supported by the U.S. National Science Foundation under Grant No. HRD-1547798 and Grant No. HRD-2111661. These NSF Grants were awarded to Florida International University as part of the Centers of Research Excellence in Science and Technology (CREST) Program. Funding for this work was provided by the Florida Department of Environmental Protection.

MANAGEMENT SUMMARY

This project assessed the use of Structure-from-Motion (SfM) photogrammetry and large-area imagery (LAIs) to enhance sedimentation monitoring and coral reef habitat evaluations near Port Everglades (PEV) and Port of Miami (POM). By utilizing high-resolution LAIs and 3D models, we quantified sediment cover, benthic composition, colony-level responses, and structural complexity across reef habitats.

Sediment-associated habitats were prevalent in many surveyed areas, showing spatial variability among reef types. The Middle reef at PEV had significantly higher sand cover and lower sponge cover than other habitats, while hard coral cover remained low across all sites. These findings suggest that sediment exposure varies and may be concentrated in specific geomorphic settings, warranting consideration in future assessments. Although temporal changes over the sampling interval were limited, there was a notable increase in sand cover at POM in the second survey, indicating that LAIs sensitivity to detect small sediment changes.

Agreement between field and digital observations of sponge sediment-stress indicators was 73.2%, reinforcing the reliability of LAIs. Coral responses varied, with reduced growth probability and greater shrinkage observed in some PEV habitats, whereas POM colonies exhibited more stable patterns. These results should be interpreted with caution, given the short duration, but they highlight the potential of LAIs to reveal subtle changes at the colony level. Also, digital 3D rugosity metrics captured finer structural variation than field chain-and-tape methods, indicating that photogrammetric approaches are particularly valuable for monitoring subtle habitat complexity changes associated with sedimentation

SfM and LAIs present a reproducible and scalable framework that can enhance monitoring by: 1) identifying sediment “hotspots”; 2) supporting baseline and post-project monitoring; 3) providing permanent records for longitudinal analysis; and 4) integrating various metrics into a unified assessment platform. Combining these tools with existing diver-based and water-quality monitoring can improve detection of changes and inform habitat-specific management decisions for sediment-stressed reefs near ports.

EXECUTIVE SUMMARY

This project assessed the use of Structure-from-Motion (SfM) photogrammetry and high-resolution large-area imagery (LAIs) for monitoring sedimentation in coral reef habitats near Port Everglades (PEV) and Port of Miami (POM). Conducted by Florida International University (FIU), National Oceanic and Atmospheric Association, and the Florida Department of Environmental Protection, the study aimed to understand the impacts of sedimentation on reef conditions, benthic communities, and reef structure. Sedimentation is a significant concern in southeast Florida due to activities such as dredging and other coastal construction projects (e.g., beach nourishment), particularly affecting reefs near PEV and POM because of historical and ongoing projects.

To tackle these issues, monitoring plots were set up across various reef zones north of PEV and POM. Thousands of underwater photos were taken using SfM protocols to create orthomosaics and 3D models, which were used to measure benthic cover, sediment levels, coral and sponge conditions, coral growth, and rugosity. Results indicated that sand cover was prevalent across both periods, especially in Middle reefs of PEV, with low hard coral cover and variable sponge cover. Sediment cover increased at POM during the second survey period, highlighting the ability of LAIs to detect minimal changes in sand cover. Field observations and digital classifications aligned well, validating LAIs for detecting sediment stress. Coral growth varied, with reduced growth in some PEV areas, potentially due to sediment effects. This result underscores the advantage of using LAIs to obtain detailed observations of stress that are overlooked by rapid assessment protocols and biotic stress indicators.

The feasibility of using SfM-derived 3D models to measure fine-scale topographic changes due to sedimentation was evaluated by comparing field and digital rugosity measurements at two scales: macro- and micro-rugosity. While there was generally good concordance between field and digital micro-rugosity measurements, the degree of concordance varied by location and season, with greater decoupling observed at POM. The analysis of variance revealed that the poor agreement between methods was largely driven by the POM observations. These results indicate that field chain-and-tape and digital photogrammetric measurements of rugosity, at both micro- and macro-scales, should not be treated as interchangeable indices of reef structural complexity. Although the two methods track partially overlapping aspects of reef surface structure, the digital measurements discriminate more finely among reef types and resolve greater within-transect heterogeneity.

The project concluded that SfM photogrammetry and LAIs offer a practical framework for monitoring the impacts of sedimentation on coral reefs. These methods enhance existing monitoring by providing permanent digital records, improving spatial resolution, and enabling repeated assessments of reef changes. Incorporating these techniques can improve adaptive management and sediment-related impact assessments resulting from dredging and coastal activities in southeast Florida's coral reef by enabling scalable, repeatable measurements that are difficult to achieve with standard procedures.

TABLE OF CONTENTS

SECTION I – PROJECT OVERVIEW

1.1 Background

Southeast Florida's coral reefs are increasingly affected by sediment dynamics resulting from port infrastructure, shoreline modifications, and large-scale coastal construction projects, such as dredging at Port Everglades and the Port of Miami (Walker et al. 2012; Serrano et al., 2026). These activities can affect nearby reef habitats through direct sediment deposition, increased turbidity, and localized changes in benthic topography. Consequently, this can have significant implications for coral health, benthic community composition, and key ecosystem functions such as filtration and carbon accretion. Although the National Oceanic and Atmospheric Administration (NOAA) and state partners engage in extensive water quality and diver-based benthic monitoring to support Essential Fish Habitat (EFH) and Endangered Species Act (ESA) Section 7 related projects, these efforts often fail to capture fine-scale sediment accumulation, three-dimensional habitat structures, or biologically relevant functional responses at the spatial and temporal scales necessary for effective adaptive management around port channels.

This project builds on prior efforts supported by the NOAA's Coral Reef Conservation Program (CRCP), including projects 31240 (Develop Sediment Depth Thresholds for EFH and ESA Consultations) and 33129 (Adaptive Management Planning for Large-scale Port Dredging in Florida), which involved diver-based rapid assessments of sediment deposition and coral stress near Port Everglades. Previous studies have demonstrated that unconsolidated sediments can accumulate unevenly across reef surfaces (e.g., Serrano et al. 2026, Guzman et al. 2026), leading to localized coral stress that is not readily detected by turbidity metrics alone. Simultaneously, NOAA has conducted near-real-time water-quality monitoring for the Port Everglades deepening project since FY21, providing valuable insights into suspended sediments and turbidity, although limited in addressing benthic-scale deposition and structural changes. Consequently, NOAA and Florida International University (FIU) collaborated on this project to assess the relationships among diver-based observations, instrument-based water quality data, and fine-scale 3D mapping. This assessment aims to evaluate the impacts of sedimentation on coral reef habitats and benthic taxa that may be affected by dredging operations.

Structure-from-Motion (SfM) is a widely used remote-sensing photogrammetry technique that reconstructs high-resolution three-dimensional (3D) models from overlapping two-dimensional imagery. In coastal and marine systems, SfM has rapidly become a cornerstone tool for quantifying habitat structure, benthic composition, and geomorphic change across ecologically relevant spatial and temporal scales (Ferrari et al., 2016; Fukunaga et al., 2019). Fine-scale mapping also captures local variability in biotic cover and relevant physical features at the colony scale (0.1–1 cm pixel), which is often crucial for local management efforts (Royer et al., 2018; Simmons et al., 2022). For instance, large-scale monitoring efforts such as NOAA's National Coral Reef Monitoring Program (NCRMP) use SfM-derived orthomosaics and digital elevation models (DEMs) to extract coral demographic metrics, including colony size, density, and condition, while creating permanent digital records for long-term reef assessment (Couch et al., 2021). Similarly, SfM photogrammetry has been successfully applied to temperate rocky reefs, where diver-generated photomosaics enable quantification of macroalgal cover, invertebrate densities, and community composition with accuracy comparable to traditional field surveys but with greater spatial coverage (Spyksma et al., 2022).

At fine spatial resolutions (millimeter- to centimeter-scale), SfM captures biologically meaningful variation in benthic cover and structural complexity, key drivers of biodiversity, trophic interactions, and ecosystem resilience (Rivas et al., 2026). Recent studies have demonstrated how SfM-derived metrics (e.g., rugosity, vector ruggedness, and fractal complexity) can link benthic assemblages to habitat structure across environmental gradients in coral reef systems (Edwards et al., 2017; Wu et al., 2025). Also, SfM is increasingly used to quantify sediment dynamics and coastal morphodynamics, including shoreline change, sediment budgets, and seabed elevation variability through time using repeat DEMs, as well as estimate sediment transport in dredging channels, fluvial plains, and riverbeds (Stojic et al., 1998; Dietrich, 2015, David et al., 2021; Carvalho & Reef, 2022). In reef environments, this approach enables direct coupling of topographic change with ecological responses, allowing researchers to assess how sediment transport, deposition, and resuspension influence benthic communities. Such capabilities are particularly valuable in turbid or sediment-stressed systems, where sedimentation can modify substrate stability, light availability, and organism performance.

In this project, we applied a similar SfM approach to observe and quantify sediment stress on reef biota and changes in seabed topography in reef habitats near Port Everglades and the Port of Miami. These data will strengthen the baseline characterization of coral reef habitats around these port channels and improve impact assessments associated with dredging activities, ultimately enhancing our understanding of sediment-driven changes in reef ecosystem structure and function.

1.2 Project Goals and Tasks

The goal of this project was to demonstrate the utility of high-resolution large-area images (LAIs) to quantify potential sedimentation impacts on coral reef habitats/species (e.g., changes in bottom cover of hard bottom vs. sand) and the three-dimensional framework of the seabed (i.e., sediment accumulation and propagation) to assess baseline sedimentation characteristics across reef habitats surrounding Port Everglades and Port of Miami. Specifically, a series of large-area images from SfM were created across sites north of both ports during two time points (December-January and March-April) to:

1) Quantify differences in the percent cover of functional benthic groups in relation to unconsolidated sediments across reef types.
2) Quantify seasonal changes in the percent cover of functional benthic groups in relation to unconsolidated sediments.
3) Compare measurements of biotic stress indicators collected from *in-situ* and digital observations from large-area images.
4) Determine any changes in coral colony size in relation to sediment cover.
5) Test the feasibility of measuring fine-scale topographic variation within 3D models.

To attain these goals, we performed activities under four primary tasks:

Task 1: Quality Assurance Plan and Reporting

Task 2: Delineation and sampling of plots to assess sedimentation effects via photogrammetry

Task 3: Construction of large-area images and 3D models using Structure-from-Motion software

Task 4: Test the feasibility of large-area images and 3D models to assess spatiotemporal sedimentation effects on benthic functional groups and fine-scale topographic features.

This final report includes details only on the activities and outputs under Tasks 2–4, particularly the reporting for Task 4, which presents the results of analyses assessing how LAIs and 3D models can be used to quantify the effects of sedimentation on reef systems.

SECTION II – METHODS

2.1 Project Location and Plot Delineation (Task 2)

One site north of Port Everglades (PEV) and the Port of Miami (approximately 500 m from the channel) at each of the four main reef habitat types (Nearshore Ridge Complex, Inner, Middle, and Outer reefs) was used to quantify spatial differences in sediment cover and sedimentation effects (**Fig. 1 - 3**). These sites were chosen to match a subset of the survey locations used in the 2017-2023 diver-based surveys conducted by NOAA at each port to assess indicators of sediment stress in benthic taxa (described in Serrano et al. 2026). At each site, three 10 × 10 m plot replicates were delineated at least 10 m apart. The delineation consisted of marking each corner with masonry nails and a rebar with a submerged buoy at the southwest corner of each plot (**Fig. 4**). Also, 9 × 9 cm markers were placed at each corner of each plot to facilitate georeferencing and co-registration of large-area images from different time points (December-January vs March-April), for a total of 42 LAIs.

Sampling of Plots to Assess Sedimentation Effects Via Photogrammetry (Task 2)

After delineating the plots at each location, *in situ* measurements of sediment depth, rugosity, and biotic stress indicators were collected in each plot to compare with digital observations and measurements from LAIs and 3D models. The *in-situ* observations were conducted at two scales: the plot or transect scale (macro-scale) and the patch or quadrat scale (micro-scale). The observations at the plot or macro-scale were performed along two transects (North and South transect), laid out between semi-permanent markers placed towards the center of the plot. Within each transect replicate, rugosity, sediment depth, and biotic stress indicators in association with sedimentation were measured and annotated. Rugosity at the macro-scale was estimated using the chain-and-tape method by calculating the ratio of the length of a flexible chain laid out along the reef topography and the total length of the transect (~10 m running east to west of the plots). The biotic stress indicators were collected following Serrano et al. (2026) by classifying benthic functional group sediment stress into 5 categories/indices: no visual stress, sediment accumulation, buried tissue, sediment halos, and recent partial mortality. We classified the sediment stress of corals, gorgonians, and sponges intercepted by the transect line. At the micro-scale, only rugosity measurements were performed using chain-and-tape methods along three randomly placed mini-transects (50 cm each) at each of the four corners of the plots (i.e., measurements within a 50 cm x 50 cm quadrat).

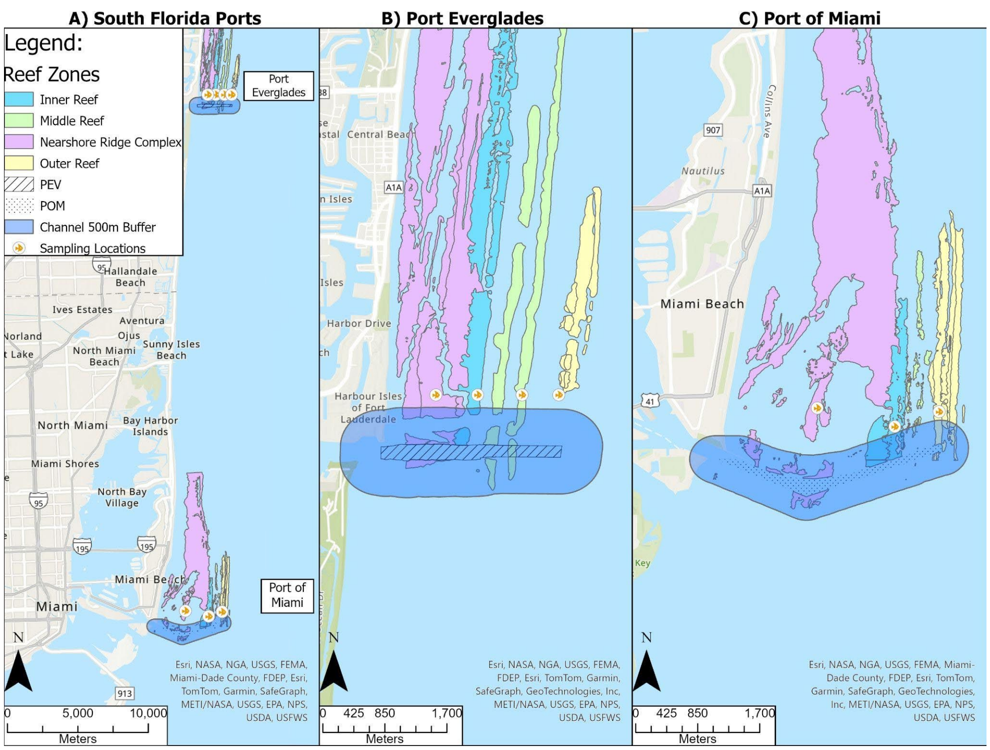

Figure 1: *Map of Port Everglades (PEV) and Port of Miami (POM) sites. The blue area represents a 500 m buffer around the ports.*

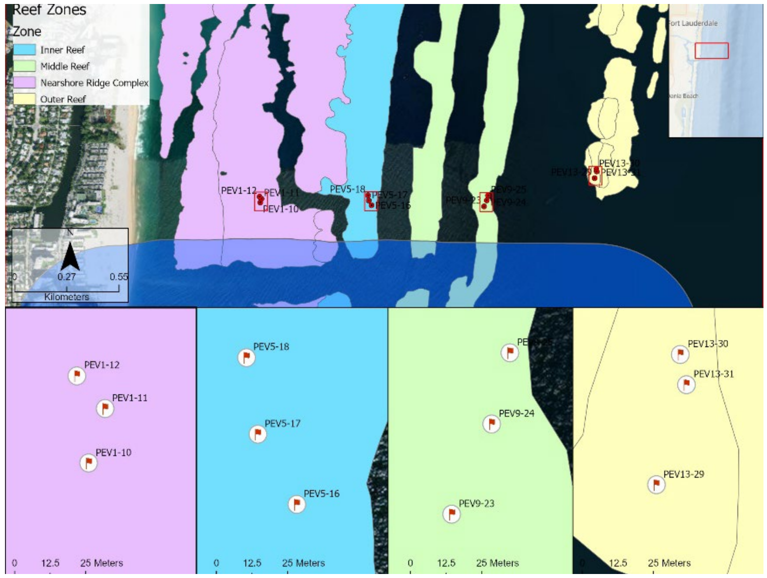

Figure 2: *Map of the sites selected in Port Everglades (PEV). Three 10 x 10 m replicate plots were established at each sampling location (orange fish symbol). Blue polygon represents a 500 m buffer around the ports. Reef types represented as (from Nearshore Complex to offshore): Nearshore Complex – pink, Inner Reef – light blue, Middle Reef – green, and Outer Reef (yellow).*

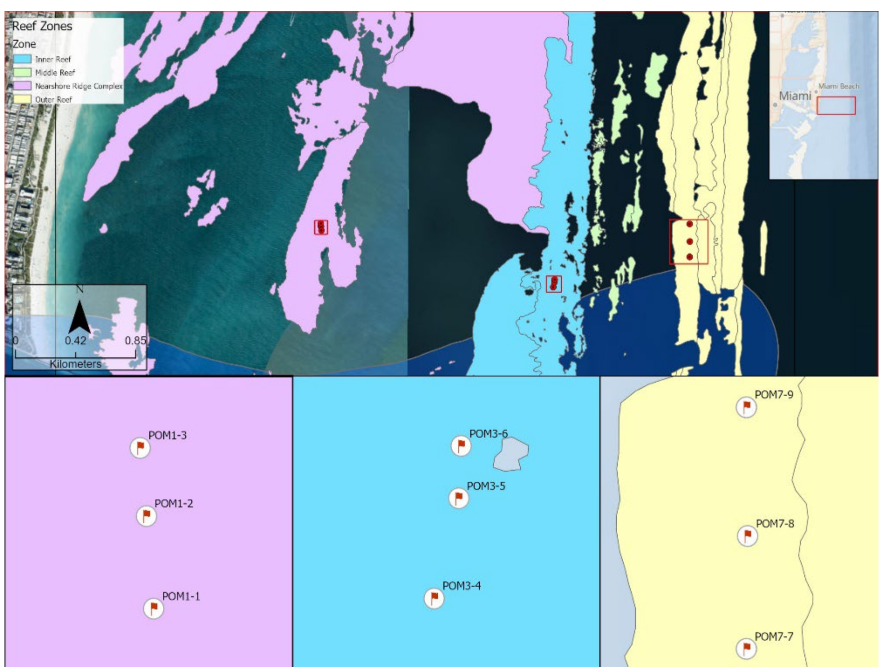

Figure 3: *Map of the sites selected in Port of Miami (POM). Three 10 x 10 m replicate plots were established at each sampling location (orange fish symbol). Blue polygon represents a 500 m buffer around the ports. Reef types represented as (from Nearshore Complex to offshore): Nearshore Complex – pink, Inner Reef – light blue, and Outer Reef (yellow).*

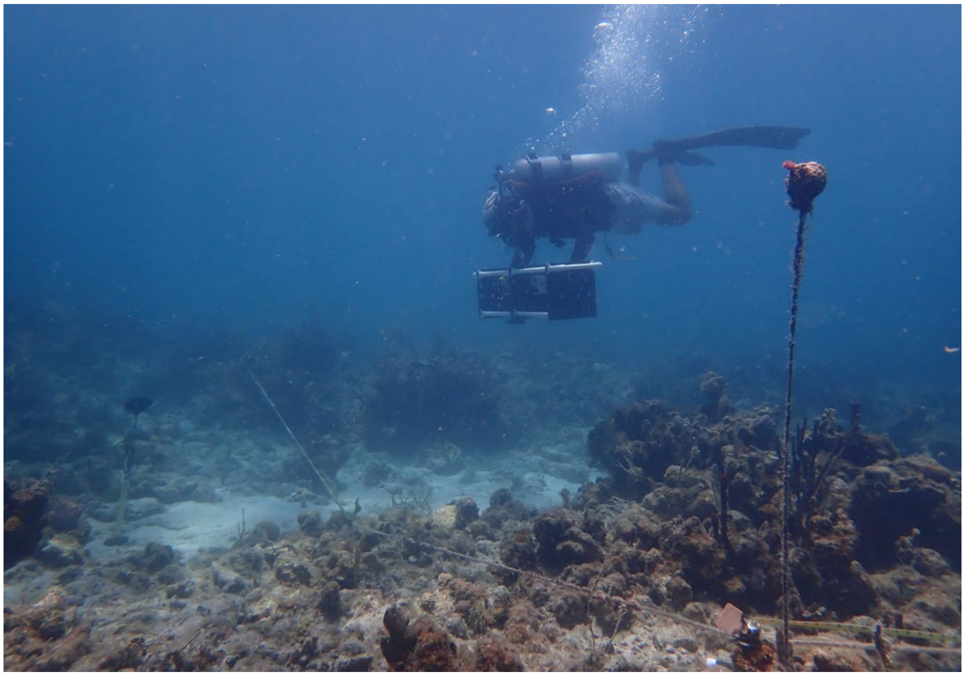

Figure 4: *Example of a photomosaic being conducted in a plot delineated by masonry nails and a submersible buoy.*

In the field, we collected benthic digital images following NOAA's guidelines for creating LAIs of tropical, shallow-water coral reefs (Cook et al., 2023). This photogrammetric methodology consisted of photographing the space delineated by the 10m x 10m plots every second using Nikon D7500 DSLR cameras equipped with wide-angle lenses to minimize distortion. Photographs were collected once per sampling period using a systematic "lawnmower" pattern with ~60%–80% overlap to ensure complete coverage and high-quality image alignment. Approximately 2,200 images were captured per plot, depending on rugosity and site complexity.

2.2 Construction of Large-Area Images (LAIs) and 3D Models Using Structure-from-Motion Software (Task 3)

Back in the laboratory, after the photographs were collected, all images were reviewed for sharpness and clarity before processing. Images were color-corrected using Adobe Lightroom and subsequently uploaded into Agisoft Metashape Pro (Structure-from-Motion software), where they were aligned. Following alignment, dense point clouds were generated using the high-quality depth-mapping settings. These dense clouds were then used to construct 3D meshes (models) and LAIs, providing structural and planar representations of the reef. To process the information within the LAIs, these were split into 1 m x 1 m quadrats using ArcGIS Pro functions to quantify the percent cover of benthic functional groups (**Figure 5A-B**). The dense point clouds were exported in. ply format and uploaded into UCSD's VISCORE software for scaling and co-registration across time points to estimate micro- and macro-rugosity from the 3D models and ortho-project LAIs to measure the size of coral colonies (Petrovic et al., 2014) (**Figure 5C**). Scaling was based on known distances recorded *in-situ* with eight 0.5 m scale bars, at which depth was also recorded.

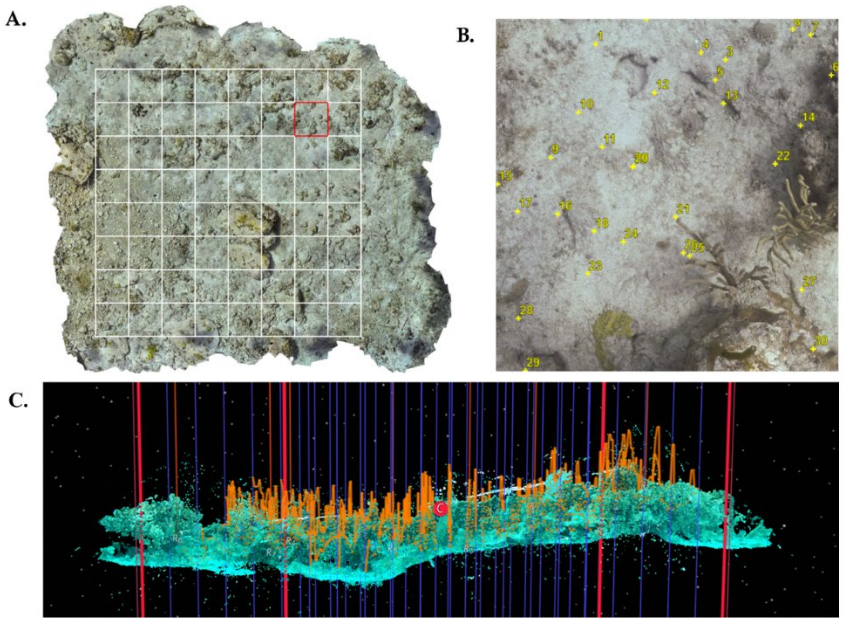

Figure 5: *A) Screenshot of Large Area Image (LAI) being segmented into smaller 1 m^2 photo quadrats for point count analysis. B) Screenshot of CoralNet interface with random points overlaid for identification. C) Screenshot of VISCORE program processing rugosity metrics.*

2.3 Assessment of the Feasibility of SfM Spatiotemporal Analysis of Sedimentation Effects (Task 4)

We quantified the percent cover of sediment and key benthic functional groups (corals, algae, sponges) within each plot and across all survey periods using annotated LAIs. To do this, the 1 × 1 m digital quadrats extracted from each LAI using ArcGIS were uploaded to CoralNet (Figure 5B), where we trained a machine-learning-based classifier to assist with point identification (Chen et al., 2021). We used 60%–75% of the quadrats to train the CoralNet classifier model to estimate the percent cover of the benthic functional groups. This percent cover data was used to assess how sediment prevalence differed across reef types and ports and influenced benthic community structure. Differences in the percent cover of corals, macroalgae, sponges, and other functional groups in relation to sediment prevalence were evaluated across reef types using generalized linear mixed models (GLMMs). The project was intended to capture seasonal dynamics of sediment and benthic cover changes across the wet and dry season; however, due to permitting issues that delayed the project, we were only able to compare benthic groups across two close time points (December-January, March-April).

We also compared the biotic stress indicators, such as partial mortality and sediment smothering, between *in-situ* field observations and annotated large-area images. *In-situ* and LAI observations were matched using the unique location of the benthic colonies along the plot transects used for field rugosity and stress indicator measurements. This allowed the building of contingency table with a corresponding Chi^2 test to assess the correspondence of the field and digital observations. Additionally, GLMMs were used to test the relationship between sediment depth/accumulation and stress indicators. This helped evaluate the effectiveness of digital tools in detecting sediment-related stress responses and improved confidence in remote monitoring techniques.

Orthoprojected LAIs and scaled 3D models from VISCORE were used to estimate changes in colony size and fine-scale topography due to sedimentation. High-resolution orthoprojected LAIs were then exported from VISCORE to correct geometric distortions during coral delineation. These orthoprojected LAIs were processed in TagLab, an AI-assisted annotation software developed by the Italian National Research Council (Pavoni et al., 2022). TagLab was used to delineate and estimate the planar area (size) of benthic features such as live coral colonies and sponges using its machine-learning tools and manual refinement, thereby creating a size-structure baseline and, potentially, estimating size changes due to sedimentation. Additionally, using rugosity indices, we tested the feasibility of using 3D models from SfM to measure fine-scale topographic changes due to sedimentation. To accomplish this, 3D models scaled in VISCORE were used to digitally measure rugosity within plot-level transects (macro-rugosity) that were used in the field. Also, we measured rugosity digitally within the 50cm x 50cm corner quadrats (micro-rugosity). A correlation test between field (*in-situ)* and digital rugosity measurements allowed us to assess the feasibility of quantifying sedimentation from SfM by evaluating how microhabitat features were influenced by sediment accumulation or erosion.

2.4 Measurement of grain size across space and time

Sediment grain-size composition was quantified from samples collected across Nearshore Complex, Inner Reef, Middle Reef, and Outer Reef zones at Port Everglades (PEV) and Port of Miami (POM) at two timepoints (T1 and T2). Samples were dry-sieved through a sequential series of mesh sizes (35, 53, 125, 250, and 500 µm), and cumulative weights were converted to non-overlapping size-class fractions expressed as proportions of total dry mass. Beta-distributed generalized linear mixed models (GLMMs) were fitted for each size class using the glmmTMB package in R, with plot identity included as a random intercept to account for repeated sampling across timepoints. Fixed effects of location, reef zone, timepoint, and their interactions were evaluated using Type II Wald chi-squared tests.

SECTION III – RESULTS

A series of statistical analyses was conducted to evaluate the effectiveness of high-resolution large-area images (LAIs) in quantifying the potential impacts of sedimentation on coral reef habitats and species. This includes examining changes in bottom cover, such as hard bottom versus sand, as well as analyzing the three-dimensional structure of the seabed, specifically sediment accumulation and propagation. While LAIs provided robust assessments of benthic cover and structural change, the approach was less effective for evaluating sediment stress on soft corals and other flexible benthic organisms. Because soft corals move continuously with water motion during image acquisition, they are often poorly reconstructed or appear blurred and distorted in the final photogrammetric products, limiting the reliability of condition assessments and fine-scale analyses for these taxa. Below, we report the main findings and interpretations from these analyses for each project goal (Task 4 – Deliverable D).

3.1 Goal 1 - Quantify differences in the percent cover of functional benthic groups in relation to unconsolidated sediments across reef types

Predicted benthic percent cover from GLMMs differed substantially among functional groups and reef habitats, with sand consistently dominating benthic composition across both Port Everglades (PEV) and Port of Miami (POM) (**Figure 6.1.1**). Hard coral cover remained uniformly low across all reefs and locations, whereas sponge and sand cover showed stronger spatial structuring, particularly in PEV.

In PEV, hard coral cover did not differ significantly among reef zones (all Tukey-adjusted $p > 0.99$), with predicted values remaining near zero across the Nearshore Complex, Inner Reef, Middle Reef, and Outer reefs (**Table 6.1.1**). In contrast, sand cover exhibited strong reef-related differences. The Middle Reef had substantially greater sand cover than all other reef zones, exceeding inner reefs by approximately 45.5% ($z = -12.46$, $p < 0.001$), Nearshore Complex reefs by 51.7% ($z = 14.85$, $p < 0.001$), and Outer reefs by 32.2% ($z = 8.82$, $p < 0.001$). The Outer Reef also had significantly greater sand cover than the inner reef ($p = 0.0028$), while Nearshore Complex and Inner Reef did not differ significantly. Predicted values indicated particularly elevated sand cover at Middle Reef (~85–90%), compared to ~35–55% across the remaining reef zones.

Sponge cover in PEV also varied significantly among reefs. The Middle Reef had significantly lower sponge cover than the inner reef (*estimate* = 10.11, $p = 0.0287$), Nearshore Complex reefs (*estimate* = −12.42, $p = 0.0020$), and Outer reefs (*estimate* = −9.81, $p = 0.0362$). No significant differences were detected among Nearshore Complex, Inner Reef, and Outer reefs. Predicted sponge cover generally ranged from approximately 5–18%, with the lowest values occurring at Middle reefs.

Patterns of the benthic functional groups in POM were comparatively weaker. Hard coral cover again showed no significant differences among reef zones (all $p > 0.99$), with predicted values remaining close to zero throughout. Sponge cover similarly did not differ significantly among reefs (all $p > 0.84$), and predicted values remained relatively consistent across Nearshore Complex, Inner Reef, and Outer reefs (~10–12%). Sand cover in POM displayed only one significant contrast, with the Outer Reef having lower predicted sand cover than Nearshore Complex reefs (*estimate* = 9.84, $z = 2.83$, $p = 0.0130$). No other sand comparisons were significant.

Overall, the benthic community was characterized by high sand cover and low hard coral cover across both locations, although reef zonation effects were more pronounced in PEV than in POM. The most distinct spatial pattern was the exceptionally high sand cover and reduced sponge cover observed at the Middle Reef in PEV.

Rest of page intentionally left blank.

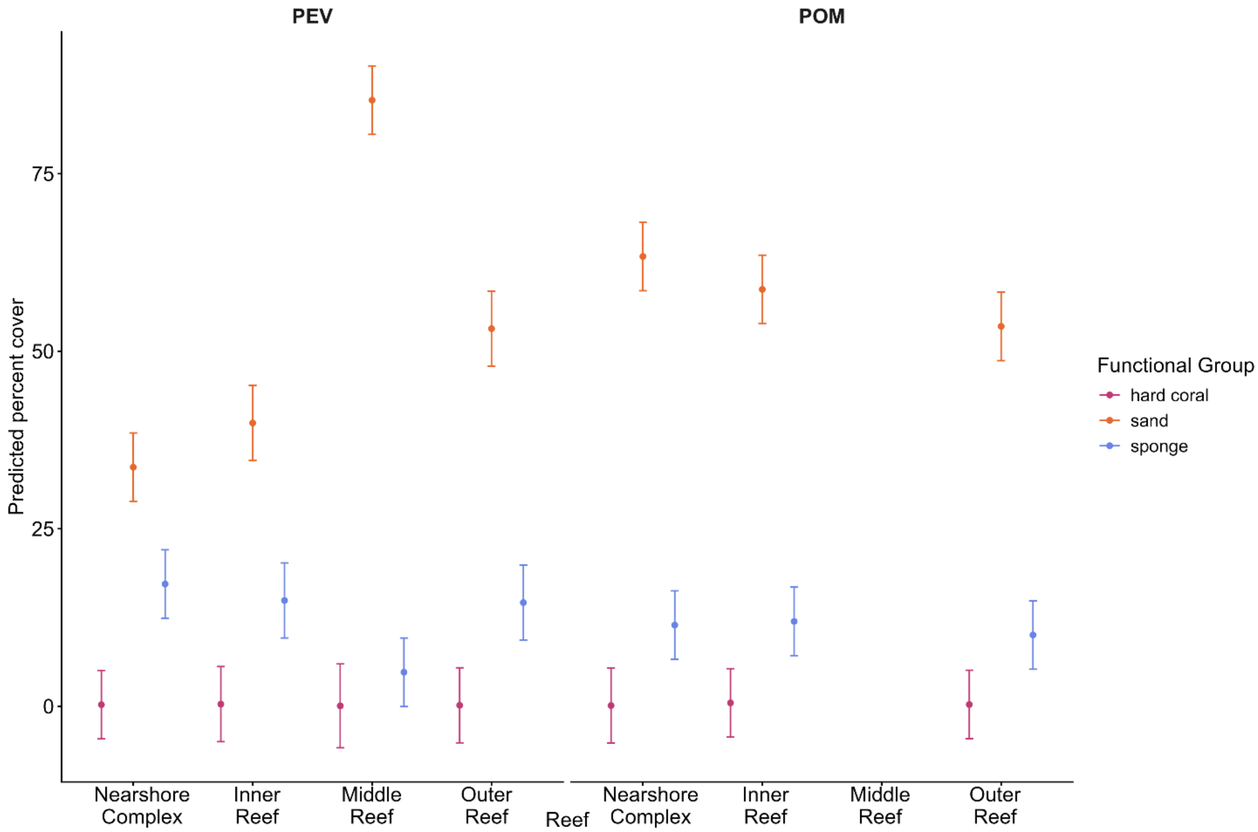

Figure 6.1.1: *Predicted percent cover (mean ± 95% confidence intervals) of hard coral, sand, and sponge functional groups across reef zones in PEV and POM derived from a Gaussian generalized linear mixed-effects model (GLMM). Reef zones included Nearshore Complex, Inner Reef, Middle Reef, and Outer Reefs, although Middle reefs were absent in POM. Sand consistently dominated benthic cover across both locations, with exceptionally high predicted cover at the Middle Reef in PEV. Sponge cover was generally lower at Middle Reef in PEV, while hard coral cover remained uniformly low across all reef zones and locations. Predictions were generated from models including the interaction between category, reef, and location, with plot included as a random effect.*

Table 6.1.1: *Tukey-adjusted pairwise comparisons of predicted percent cover among reef zones for hard coral, sand, and sponge functional groups within PEV and POM. Comparisons were derived from estimated marginal means of a Gaussian generalized linear mixed-effects model (GLMM) including the interaction between functional group, reef zone, and location, with plot treated as a random effect. Reported values include estimated differences in percent cover between reef zones, standard errors (SE), z-values, adjusted p-values, and significance levels ($p < 0.05$). Significant contrasts were primarily associated with sand and*

*sponge cover in PEV, particularly involving the Middle Reef, whereas few significant differences were detected in POM. Significance codes: p < 0.05 (), p < 0.01 **()**, **p < 0.001 ()**.*

Location	Category	Contrast	Estimate	SE	z value	p value	Sig
PEV	hard coral	Inner Reef - Middle Reef	0.246	4.044	0.061	0.9999	
PEV	hard coral	Inner Reef - Nearshore Complex	0.080	3.650	0.022	1.0000	
PEV	hard coral	Inner Reef - Outer Reef	0.168	3.813	0.044	1.0000	
PEV	hard coral	Middle Reef - Nearshore Complex	-0.166	3.891	-0.043	1.0000	
PEV	hard coral	Middle Reef - Outer Reef	-0.078	4.044	-0.019	1.0000	
PEV	hard coral	Nearshore Complex - Outer Reef	0.088	3.650	0.024	1.0000	
PEV	**sand**	**Inner Reef - Middle Reef**	**-45.464**	**3.650**	**-12.455**	**0.0000**	***
PEV	sand	Inner Reef - Nearshore Complex	6.226	3.650	1.706	0.3206	
PEV	**sand**	**Inner Reef - Outer Reef**	**-13.283**	**3.813**	**-3.484**	**0.0028**	**
PEV	**sand**	**Middle Reef - Nearshore Complex**	**51.690**	**3.480**	**14.852**	**0.0000**	***
PEV	**sand**	**Middle Reef - Outer Reef**	**32.181**	**3.650**	**8.816**	**0.0000**	***
PEV	**sand**	**Nearshore Complex - Outer Reef**	**-19.509**	**3.650**	**-5.344**	**0.0000**	***
PEV	**sponge**	**Inner Reef - Middle Reef**	**10.109**	**3.650**	**2.769**	**0.0287**	*
PEV	sponge	Inner Reef - Nearshore Complex	-2.314	3.650	-0.634	0.9211	
PEV	sponge	Inner Reef - Outer Reef	0.298	3.813	0.078	0.9998	
PEV	**sponge**	**Middle Reef - Nearshore Complex**	**-12.423**	**3.480**	**-3.569**	**0.0020**	**
PEV	sponge	Middle Reef - Outer Reef	-9.810	3.650	-2.688	0.0362	*
PEV	sponge	Nearshore Complex - Outer Reef	2.613	3.650	0.716	0.8909	
POM	hard coral	Inner Reef - Nearshore Complex	0.374	3.650	0.102	0.9942	
POM	hard coral	Inner Reef - Outer Reef	0.227	3.480	0.065	0.9977	
POM	hard coral	Nearshore Complex – Outer Reef	-0.147	3.650	-0.040	0.9991	
POM	sand	Inner Reef - Nearshore Complex	-4.633	3.480	-1.331	0.3777	

Location	Category	Contrast	Estimate	SE	z value	p value	Sig
POM	sand	Inner Reef - Outer Reef	5.207	3.480	1.496	0.2928	
POM	**sand**	**Nearshore Complex - Outer Reef**	**9.840**	**3.480**	**2.827**	**0.0130**	*
POM	sponge	Inner Reef - Nearshore Complex	0.524	3.480	0.151	0.9876	
POM	sponge	Inner Reef - Outer Reef	1.913	3.480	0.550	0.8467	
POM	sponge	Nearshore Complex - Outer Reef	1.389	3.480	0.399	0.9160	

3.2 Goal 2 - Quantify seasonal changes in the percent cover of functional benthic groups in relation to unconsolidated sediments

Predicted percent cover differed markedly among functional groups across both locations and time points (**Figure 6.2.1**). Sand consistently represented the dominant benthic component, whereas sponge cover was intermediate and hard coral cover remained uniformly low. Temporal changes in benthic composition were generally limited, with few significant differences detected between time points within functional groups and locations (**Table 6.2.1**).

In PEV, hard coral cover did not differ between time points ($p = 0.994$), with predicted values remaining near zero at both sampling periods. Sand cover declined slightly from t1 to t2, although this change was not significant (*estimate* = 4.29, $z = 0.92$, $p = 0.356$). Sponge cover showed a small increase from t1 to t2, but this pattern was also non-significant (*estimate* = −2.80, $z = -0.60$, $p = 0.547$). Predicted sponge cover in PEV increased from approximately 11% at t1 to ~14% at t2, while sand cover decreased from ~56% to ~51%.

Patterns in POM were similarly stable through time for hard coral and sponge cover. Hard coral cover remained unchanged between t1 and t2 ($p = 0.983$), and sponge cover showed no significant temporal difference (*estimate* = −3.33, $p = 0.515$). In contrast, sand cover increased significantly from t1 to t2 in POM (*estimate* = −10.49, $z = -2.05$, $p = 0.040$), corresponding to an increase in predicted sand cover from approximately 53% at t1 to ~64% at t2.

Overall, temporal variation in benthic cover was weak relative to differences among functional groups. Sand consistently dominated benthic composition across both locations and time points, while hard coral cover remained minimal throughout the study. The only significant temporal shift detected was an increase in sand cover in POM from t1 to t2.

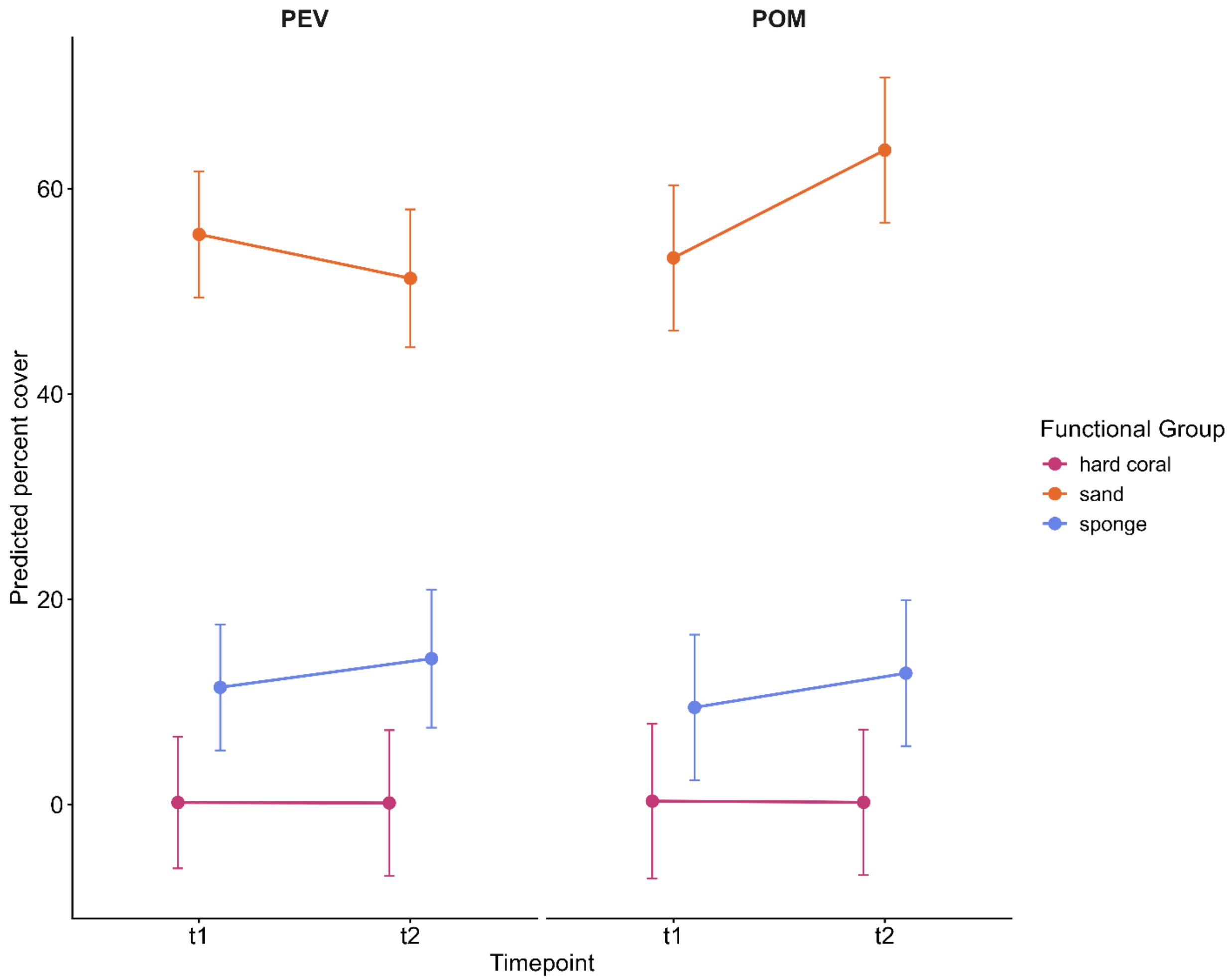

Figure 6.2.1: *Predicted percent cover (mean ± 95% confidence intervals) of hard coral, sand, and sponge functional groups across two sampling time points (t1 and t2) in PEV and POM derived from a Gaussian generalized linear mixed-effects model (GLMM). Predictions were generated from models including the interaction between functional group, timepoint, and location, with plot included as a random effect. Sand consistently dominated benthic cover across both locations and time points, while hard coral cover remained minimal. Temporal changes were generally weak, although sand cover increased in POM from t1 to t2.*

Rest of page intentionally left blank.

Table 6.2.1: *Tukey-adjusted pairwise comparisons of predicted percent cover between time points (t1 vs. t2) for hard coral, sand, and sponge functional groups within PEV and POM. Comparisons were derived from estimated marginal means of a Gaussian generalized linear mixed-effects model (GLMM) including functional group, time point, and location interactions, with plot treated as a random effect. Reported values include estimated differences in percent cover between time points, standard errors (SE), z-values, adjusted p-values, and significance levels. Most temporal contrasts were not significant, indicating relatively stable benthic composition through time; however, sand cover in POM increased significantly from t1 to t2 (p = 0.0403). Significance codes: p < 0.05 (), p < 0.01 (**), p < 0.001 ()***

Location	Category	Contrast	Estimate	SE	z value	p value	Sig
PEV	hard coral	t1 - t2	0.037	4.878	0.008	0.9939	
PEV	sand	t1 - t2	4.287	4.647	0.923	0.3562	
PEV	sponge	t1 - t2	-2.798	4.647	-0.602	0.5471	
POM	hard coral	t1 - t2	0.112	5.274	0.021	0.9831	
POM	**sand**	**t1 - t2**	**-10.493**	**5.116**	**-2.051**	**0.0403**	*
POM	sponge	t1 - t2	-3.328	5.116	-0.651	0.5154	

Rest of page intentionally left blank.

3.3 Goal 3 - Compare measurements of biotic stress indicators collected from *in-situ* and digital observations from large-area images and grain size composition

Comparison of sponge condition classifications from *in-situ* surveys and LAI photogrammetry showed strong overall agreement, particularly for the sediment accumulation sponge condition category (***Fig. 6.3.1***). After removing unknown, missing, and not-found records, a total of 164 valid paired observations were retained across both time points. Exact agreement between *in-situ* and LAI classifications occurred for 120 observations, corresponding to 73.2% overall agreement.

Agreement was highest for sponges classified as sediment accumulation (SA). Of the *in-situ* SA observations, 120 were also classified as SA using LAI, while 6 were classified as no visual stress (NVS) and none were classified as buried. This indicates that LAI reliably identified the dominant SA sponge condition category. In contrast, agreement was lower for NVS and buried classifications. Among *in-situ* NVS observations, 21 were classified as NVS by LAI, while 13 were classified as SA. For buried sponges, 4 observations were classified as buried by LAI, but none matched an *in-situ* buried classification.

Most disagreement occurred between NVS and SA categories, suggesting that LAI classifications were more likely to confuse exposed/non-sedimented sponge condition with sediment accumulation conditions than with burial. Buried classifications were rare overall, limiting interpretation of model performance for that category. Overall, the classification comparison suggests that LAI photogrammetry captured broad sponge condition patterns reasonably well, especially for the dominant SA category, but was less consistent for distinguishing NVS from SA and for detecting rare buried sponge conditions.

Grain-size composition was dominated by the coarse 250–500 μm sand fraction across all zones and locations (30–76% of total dry mass), with proportional composition varying significantly by reef zone ($\chi^2 = 29.62$, $p < 0.001$) and location ($\chi^2 = 4.93$, $p = 0.026$). Despite this coarse-sand dominance, both PEV and POM shifted toward finer grain-size compositions from T1 to T2, fine fractions increased while the coarse 250–500 μm fraction decreased significantly over time ($\chi^2 = 5.39$, $p = 0.020$). The 35–53 μm fraction showed a significant overall timepoint effect ($\chi^2 = 6.58$, $p = 0.036$), with raw means doubling at PEV (0.71% → 2.47%) and increasing more modestly at POM (2.47% → 3.26%). The very finest fraction (<35 μm) followed the same directional trend at PEV (0.045% → 0.085%), though this did not reach significance given the small absolute values and high variability. The clearest and most statistically robust signal was a significant location × timepoint interaction for the 125–250 μm fraction ($\chi^2 = 5.69$, $p = 0.017$): the two locations did not differ at T1 ($p = 0.12$), but by T2 PEV had substantially less of this mid-sized fraction than POM (odds ratio ≈ 0.48, $p < 0.001$), indicating the locations are diverging in composition over time in this size class specifically.

Reef zone was a significant structuring factor across multiple size classes, and zone-level patterns differed between locations. At the Inner Reef, POM consistently had higher proportions of fine material than PEV across the <35 μm ($p = 0.002$), 35–53 μm ($p < 0.001$), and 53–125 μm (p =

0.017) fractions, yet the two locations changed at comparable rates over time. In PEV, the most pronounced temporal change occurred at the Middle Reef, where the fine (<125 µm) fraction increased from 20.9% to 44.9% between timepoints ($p < 0.001$), the largest single zone-level shift in the data. Contrary to expectation, Nearshore Complex and Inner Reef zones were not finer than Middle and Outer Reef zones, they were in fact coarser, with Nearshore Complex sediment at PEV dominated by the 250–500 µm fraction (72–76%), while Middle and Outer reef zones accumulated more fine and medium material.

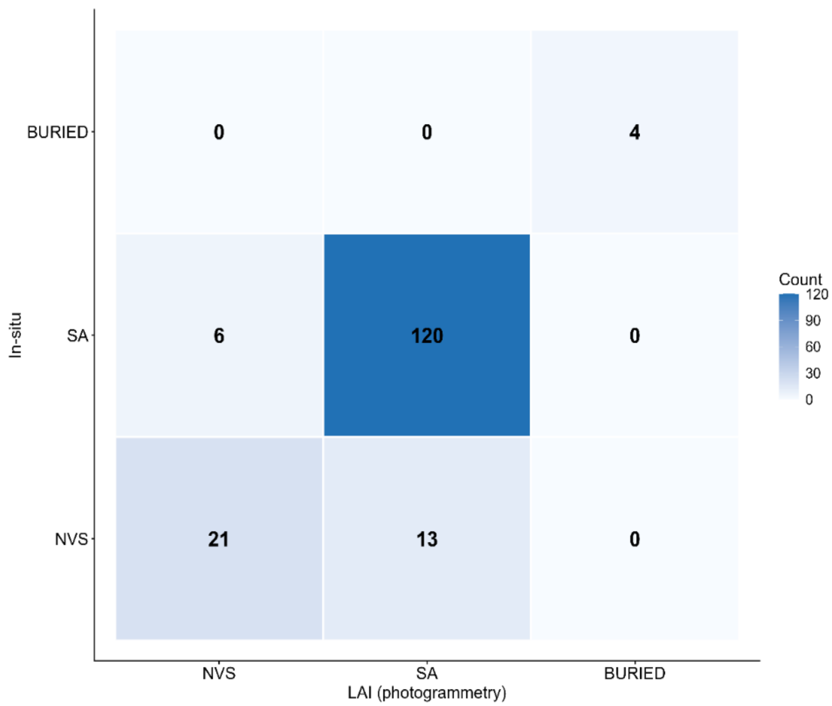

Figure 6.3.1: *Confusion matrix comparing sponge classification outcomes between in-situ observations and classifications derived from large-area imaging (LAI) photogrammetry. Values within each cell represent the number of sponge observations assigned to each category combination. Strong agreement was observed for the sediment accumulation (SA) sponge category, with 120 observations consistently classified between methods. Most classification discrepancies occurred between no visual stress (NVS) and SA categories, while buried sponge classifications were relatively uncommon. Cell shading intensity corresponds to the frequency of observations within each category pairing.*

Rest of page intentionally left blank.

3.4 Goal 4 - Determine any changes in coral colony size in relation to sediment cover

The probability of positive colony growth differed between coral and sponge colonies across reef zones and locations **(*Fig. 6.4.1)***. For corals, growth probability was generally lower in PEV than POM, and the model detected a significant positive effect of POM location relative to PEV (β = 0.919, SE = 0.305, z = 3.009, p = 0.0026) **(*Fig. 6.4.2 & Table 6.4.1 & Table 6.4.2*)**. This indicates that coral colonies in POM had higher predicted probabilities of growth overall. Within reef zones, corals had significantly lower growth probability on Inner reefs compared with Nearshore Complex reefs (β = −0.651, SE = 0.316, z = −2.059, p = 0.0395). Middle and Outer reefs were also estimated to have a lower probability of coral growth than Nearshore Complex reefs, although these differences were not statistically significant.

For sponges, growth probability did not differ significantly among reef zones or between locations. Although the predicted sponge growth probability was highest at the Middle Reef in PEV and generally near or above 0.50 in POM, uncertainty was large across reef zones, and none of the sponge model coefficients were significant. Overall, coral growth showed clearer spatial structure than sponge growth, with reduced growth probability in Inner reefs and higher growth probability in POM, whereas sponge growth probabilities were more variable and not strongly associated with reef zone or location.

Rest of page intentionally left blank.

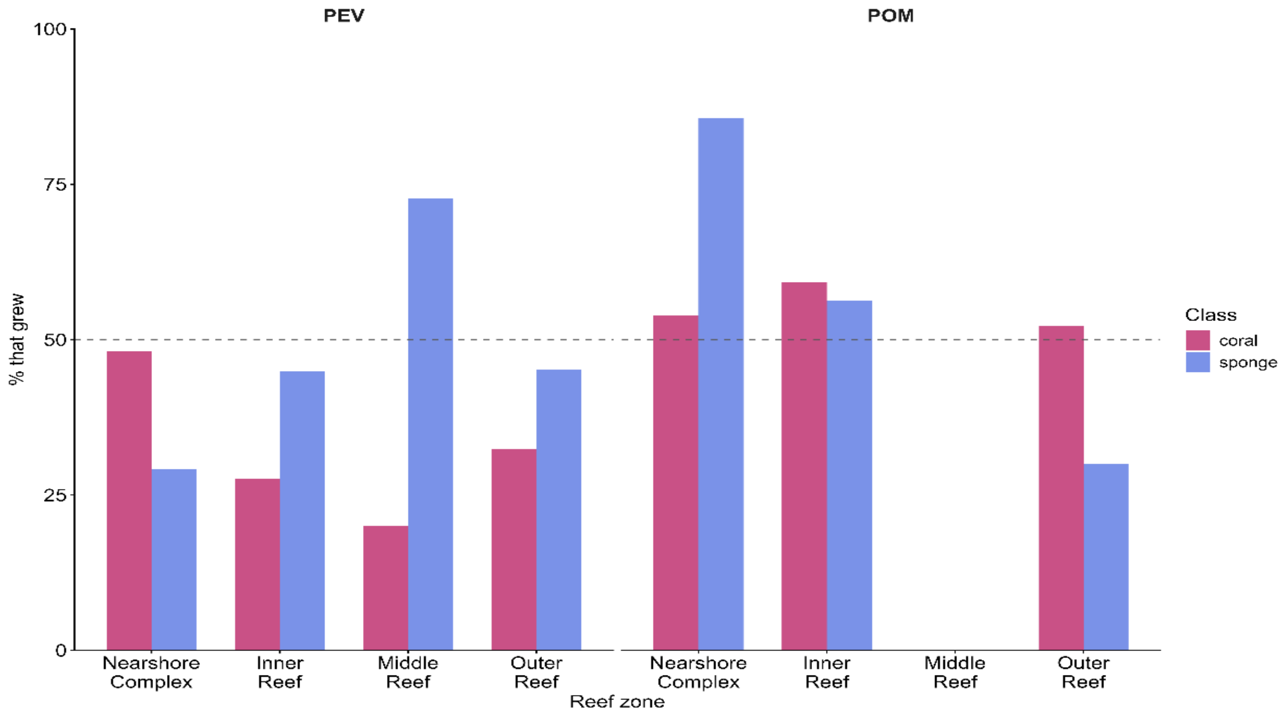

Figure 6.4.1: *Percentage of coral and sponge colonies that exhibited growth across reef zones in PEV and POM in relation to sediment-associated conditions. Bars represent the proportion of colonies classified as having increased in size between sampling periods within each reef zone and functional group. The dashed horizontal line indicates the 50% threshold, where values above the line represent most colonies exhibiting growth. Sponge colonies generally showed higher growth percentages than corals in PEV, particularly at Middle Reef, whereas coral growth exceeded sponge growth at Outer reefs in POM. No Middle Reef data were available for POM.*

Rest of page intentionally left blank.

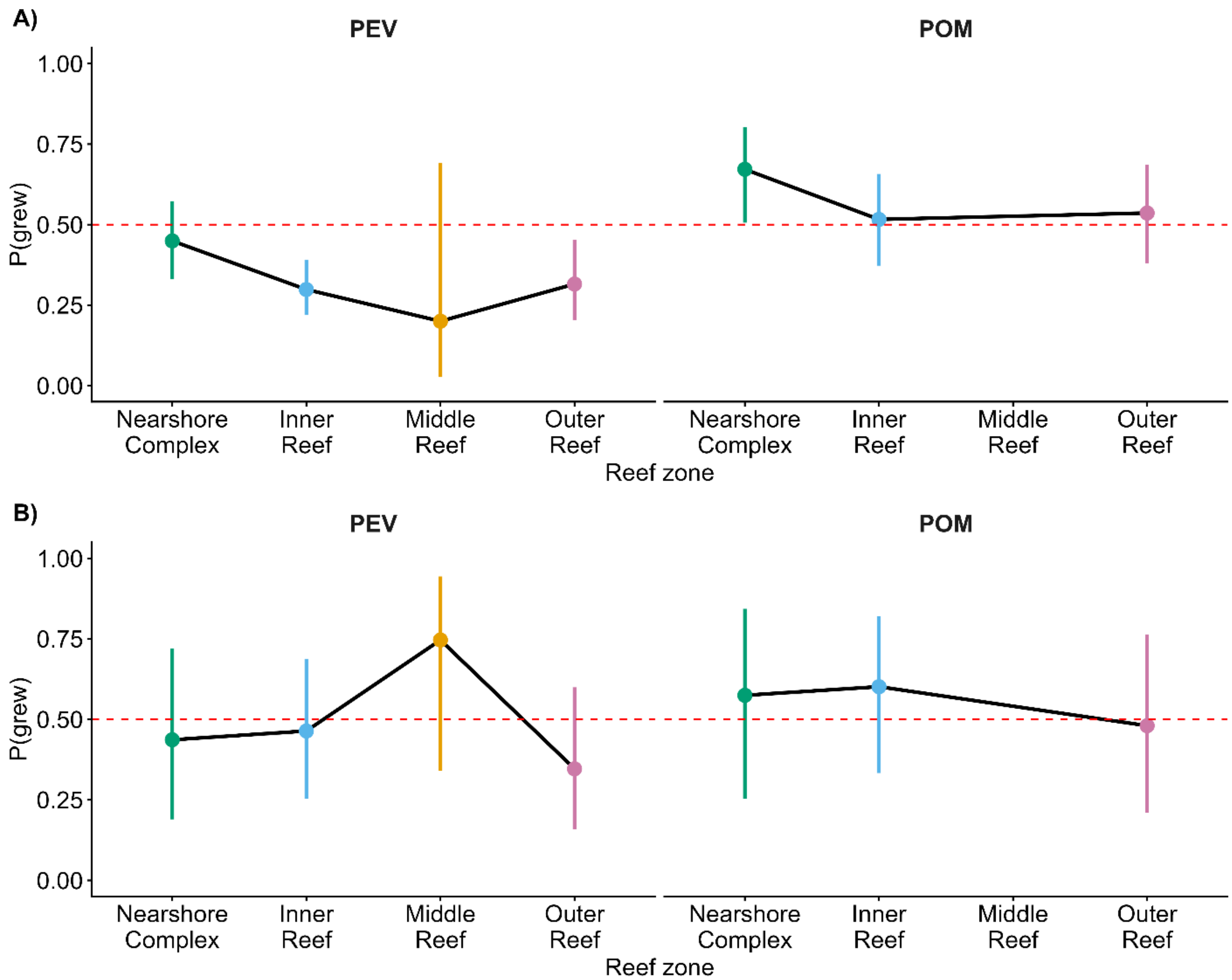

Figure 6.4.2: *Predicted probability of positive growth (mean ± 95% confidence intervals) for coral and sponge colonies across reef zones in PEV and POM derived from binomial generalized linear mixed-effects models (GLMMs). (A) Coral colony growth probability was modeled as a function of reef zone and location. Coral colonies exhibited lower predicted growth probabilities at Inner Reef and Middle Reef in PEV, while colonies in POM generally showed higher probabilities of growth across reef zones. (B) Sponge colony growth probability was modeled as a function of reef zone and location, with plot included as a random intercept. Sponge growth probabilities were more variable among reef zones, particularly in PEV, but confidence intervals broadly overlapped among locations and reef zones. Dashed horizontal lines indicate a growth probability of 0.50, where values above the line represent most colonies exhibiting positive growth. No Middle Reef data were available for POM.*

Table 6.4.1: *Results of Type II Wald chi-square tests from binomial generalized linear mixed-effects models evaluating the effects of reef zone and location on the probability of organism growth (grew). Coral growth was modeled using a binomial generalized linear model with reef and location as fixed effects (grew ~ reef + location), while sponge growth was modeled using a binomial generalized linear mixed-effects model that additionally included plot as a random intercept to account for spatial non-independence among observations within plots (grew ~ reef + location + (1 | plot)).*

Model	Predictor	Chi-square	df	p-value	
Coral growth	Reef	4.945	3	0.176	
	Location	9.056	1	0.003	**
Sponge growth	Reef	2.764	3	0.429	
	Location	0.892	1	0.345	

Table 6.4.2: *Fixed-effect coefficient estimates from binomial generalized linear mixed-effects models (GLMMs) evaluating the probability growth for coral and sponge colonies across reef zones and locations. Coral growth probability was modeled as a function of reef zone and location, while sponge growth probability was modeled as a function of reef zone and location, with plot included as a random intercept. Reported values include parameter estimates on the logit scale, standard errors (SE), z-values, and associated p-values. Coral colonies exhibited significantly lower growth probability at Inner Reefs relative to Nearshore Complex reefs and significantly higher growth probability in POM compared to PEV, whereas no significant reef zone or location effects were detected for sponge growth probability.*

Coral	Reef Zone	Estimate	Std. Error	z value	p value
	Intercept	-0.203	0.254	-0.800	0.4239
	Inner Reef	-0.651	0.316	-2.059	0.0395
	Middle Reef	-1.183	1.147	-1.032	0.3021
	Outer Reef	-0.572	0.374	-1.528	0.1265
	POM location	0.919	0.305	3.009	0.0026

Sponge	Reef Zone	Estimate	Std. Error	z value	p value
	Intercept	-0.255	0.611	-0.417	0.6766
	Inner Reef	0.110	0.716	0.154	0.8775
	Middle Reef	1.335	1.073	1.244	0.2135

Sponge	Reef Zone	Estimate	Std. Error	z value	p value
	Outer Reef	-0.380	0.777	-0.489	0.6250
	POM location	0.556	0.589	0.944	0.3450

Predicted coral log growth varied among reef zones, whereas sponge log growth remained relatively consistent between locations (***Fig. 6.4.3***). Coral colonies generally exhibited negative or near-zero log growth across reef zones, with the strongest declines observed at Middle reefs in PEV. Sponge log growth remained close to zero in both locations, indicating relatively stable colony size through time.

For corals, the reef zone significantly influenced predicted log growth (***Table 6.4.2***). Relative to Nearshore Complex reefs, coral colonies exhibited significantly lower log growth at Inner reefs ($\beta = -0.092$, SE = 0.035, $z = -2.63$, $p = 0.0085$) and Middle Reef ($\beta = -0.241$, SE = 0.095, $z = -2.53$, $p = 0.0113$). Outer reefs did not differ significantly from Nearshore Complex reefs ($p = 0.533$). Although coral colonies in POM generally exhibited slightly higher predicted log growth than colonies in PEV, the overall location effect was not significant ($p = 0.806$). Likewise, reef zone × location interaction terms were not significant, although the interaction for Inner reefs approached significance ($p = 0.094$), suggesting potential differences in reef-specific growth patterns between locations.

Model predictions indicated that coral colonies in PEV experienced the greatest declines in growth at Middle reefs, where predicted log growth values were strongly negative. In contrast, coral colonies in POM generally maintained growth values near zero across reef zones, with confidence intervals overlapping zero in most cases. These patterns suggest greater coral shrinkage or reduced growth in PEV relative to POM, particularly at Middle reefs.

For sponges, no significant effect of location on predicted log growth was detected ($\beta = 0.005$, SE = 0.039, $z = 0.137$, $p = 0.891$) (**Table 6.4.3)**. Predicted sponge log growth values remained close to zero in both PEV and POM, with broad overlapping confidence intervals indicating limited spatial variation in sponge growth dynamics. Overall, sponge colonies appeared comparatively stable through time, whereas coral colonies exhibited stronger reef-associated declines in growth, particularly within Inner Reef and Middle Reef habitats.

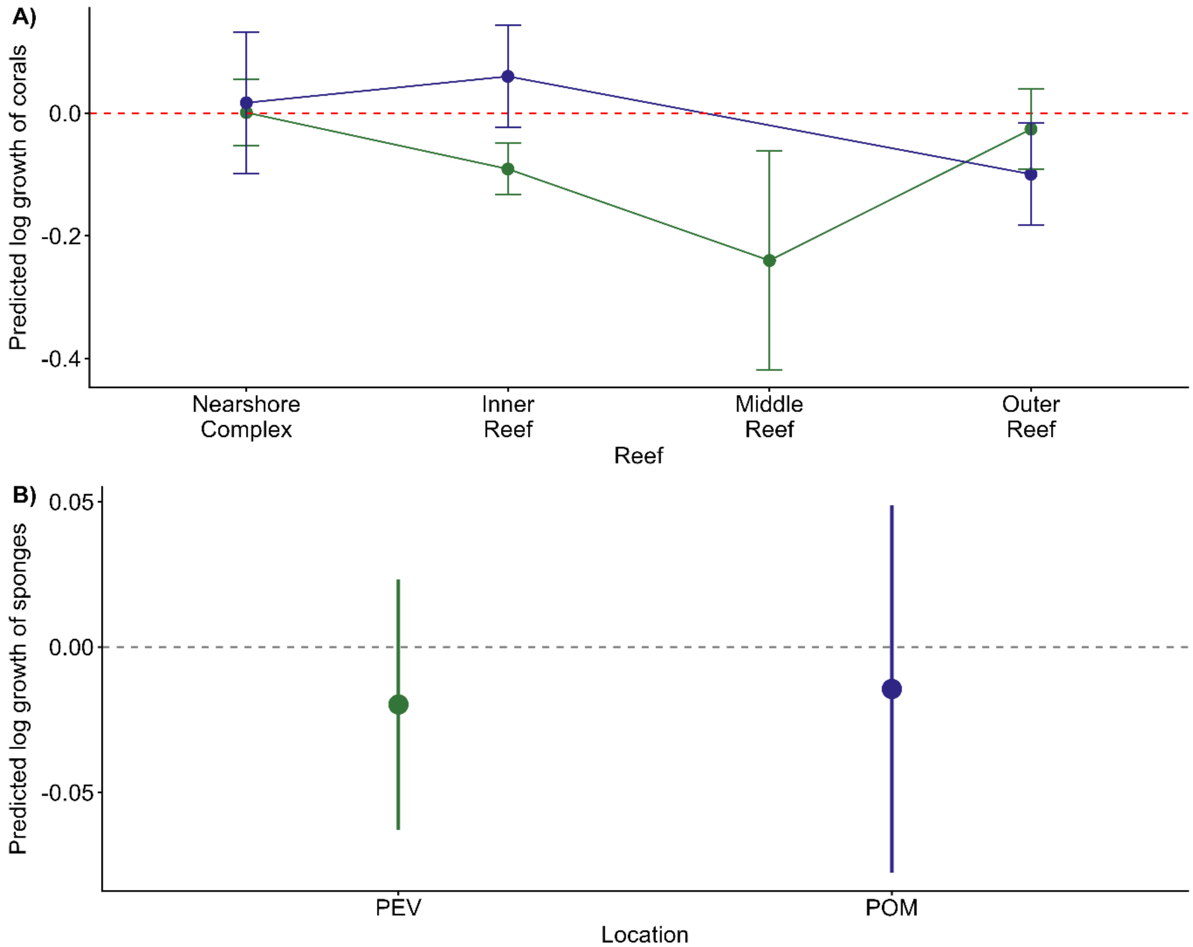

Figure 6.4.3: *Predicted log growth (mean ± 95% confidence intervals) of coral and sponge colonies derived from generalized linear mixed-effects models. (A) Predicted coral log growth across reef zones in PEV and POM. Coral colonies in POM generally exhibited higher predicted growth than colonies in PEV, particularly at Inner reefs, while Middle reefs in PEV showed the lowest predicted coral growth. No Middle Reef data were available for POM. (B) Predicted sponge log growth by location. Sponge growth remained near zero in both locations, with overlapping confidence intervals indicating limited differences between PEV and POM. Dashed horizontal lines indicate zero growth, where values above zero represent growth and values below zero represent negative growth or shrinkage.*

Table 6.4.3: *Fixed-effect parameter estimates from a Gaussian generalized linear mixed-effects model (GLMM) evaluating coral log growth across reef zones and locations. Coral log growth was modeled as a function of reef zone, location, and their interaction, with plot included as a random intercept. Reported values include parameter estimates, standard errors (SE), z-values, and associated p-values. Coral growth was significantly lower at inner reefs relative to Nearshore Complex reefs and significantly greater in POM compared to PEV. Negative log growth values indicate colony shrinkage, whereas positive values indicate colony growth.*

term	Estimate	Std. Error	z value	p value
(Intercept)	0.001	0.028	0.033	0.9733
Inner Reef	-0.092	0.035	-2.630	0.0085
Middle Reef	-0.241	0.095	-2.534	0.0113
Outer Reef	-0.027	0.043	-0.623	0.5334
Location: POM	0.016	0.065	0.246	0.8057
Inner Reef:location: POM	0.135	0.080	1.676	0.0937
Middle Reef:location: POM				
Outer Reef:location: POM	-0.089	0.085	-1.058	0.2903

Table 6.4.4: *Fixed-effect parameter estimates from a Gaussian generalized linear mixed-effects model (GLMM) evaluating predicted sponge log growth between locations. Sponge log growth was modeled as a function of location. Reported values include parameter estimates, standard errors (SE), z-values, and associated p-values. No significant differences in sponge log growth were detected between PEV and POM, indicating relatively stable sponge growth patterns across locations. Negative log growth values indicate sponge shrinkage, whereas positive values indicate sponge growth.*

term	Estimate	Std. Error	z value	p value
(Intercept)	-0.020	0.022	-0.898	0.3689
Location:POM	0.005	0.039	0.137	0.8910

3.5 Goal 5 - Test the feasibility of measuring fine-scale topographic variation within 3D models

We evaluated the feasibility of using SfM-derived 3D models to measure fine-scale topographic changes due to sedimentation by estimating rugosity indices both in the field (*in-situ*) and digitally. To achieve this, we used 3D models scaled in VISCORE for digital rugosity measurements and collected *in-situ* rugosity data using the chain-and-tape method. Both types of rugosity measurements were conducted at two scales: the plot or transect scale (macro-rugosity hereafter) and the patch or quadrat scale (micro-rugosity hereafter). We then correlated the field and digital rugosity measurements at both macro (observations spanning several meters) and micro (observations spanning submeters) scales. This analysis aimed to understand how microhabitat features and topographic characteristics varied across spatial scales of structural complexity and to identify the scale at which comparison between the two methods is feasible. Below are the results of the rugosity at the micro- and macro-scales:

3.5.1 Correlation of field and digital rugosity at the micro-scale (submeter observations)

3.5.1.1 Correlation analysis to assess the concordance

In general, there was a concordance between field and digital micro-rugosity measurements – i.e., the slopes across comparisons were not different from the 1:1 correlation slope; however, the strength of the concordance was dependent on the location (ports) and season (time points) of the observations (***Fig. 6.5.1***). At Port Everglades (PEV), across both time points, there was a positive relationship between field and digital observations (Table 6.5.1, $R^2 = 0.12–0.22$), and neither slope significantly deviated from 1. However, the low R^2 values and weak p-values, such as at the second time point (t2), suggest that spatial and temporal factors may amplify the differences between field and digital observations. In contrast, the level of decoupling between observations was higher in the plots located north of the Port of Miami (POM) (***Fig. 6.5.1**, **Table 6.5.1***). The highest decoupling in POM also occurred at the second time point, as indicated by a significant slope different from 1 ($p = 0.015$) and a very small R^2 ($R^2 = 0.006$), suggesting that both methods explain very little shared variance. Also, at the first time point, R^2 was small ($R^2 = 0.037$), even though the slope is statistically consistent with 1 (***Table 6.5.1***), again suggesting a reduced share of variance.

Table 6.5.1: *Summary of linear models assessing the concordance between field and digital rugosity measurements at the micro-scale (within submeter quadrats). For both locations (PEV – Port Everglades, POM – Port of Miami) and time points (t1 – first time point, t2 – second time point), the table includes the coefficient of variance or determination (R²) and slope between field and digital rugosity measurements, and the t-statistic (t (vs. 1:1)) and p-values (p (vs. 1:1)) associated with testing the difference between the observed slope and the 1:1 expected slope.*

Location	Time point	R^2	Slope	Slope SE	t (vs. 1:1)	*p* (vs. 1:1)
PEV	t1	0.122	1.636	0.713	0.892	0.378

Location	Time point	R²	Slope	Slope SE	t (vs. 1:1)	*p* (vs. 1:1)
PEV	t2	0.224	2.275	0.705	1.808	0.079
POM	t1	0.037	0.915	0.850	-0.100	0.921
POM	t2	0.006	0.136	0.330	-2.615	0.015

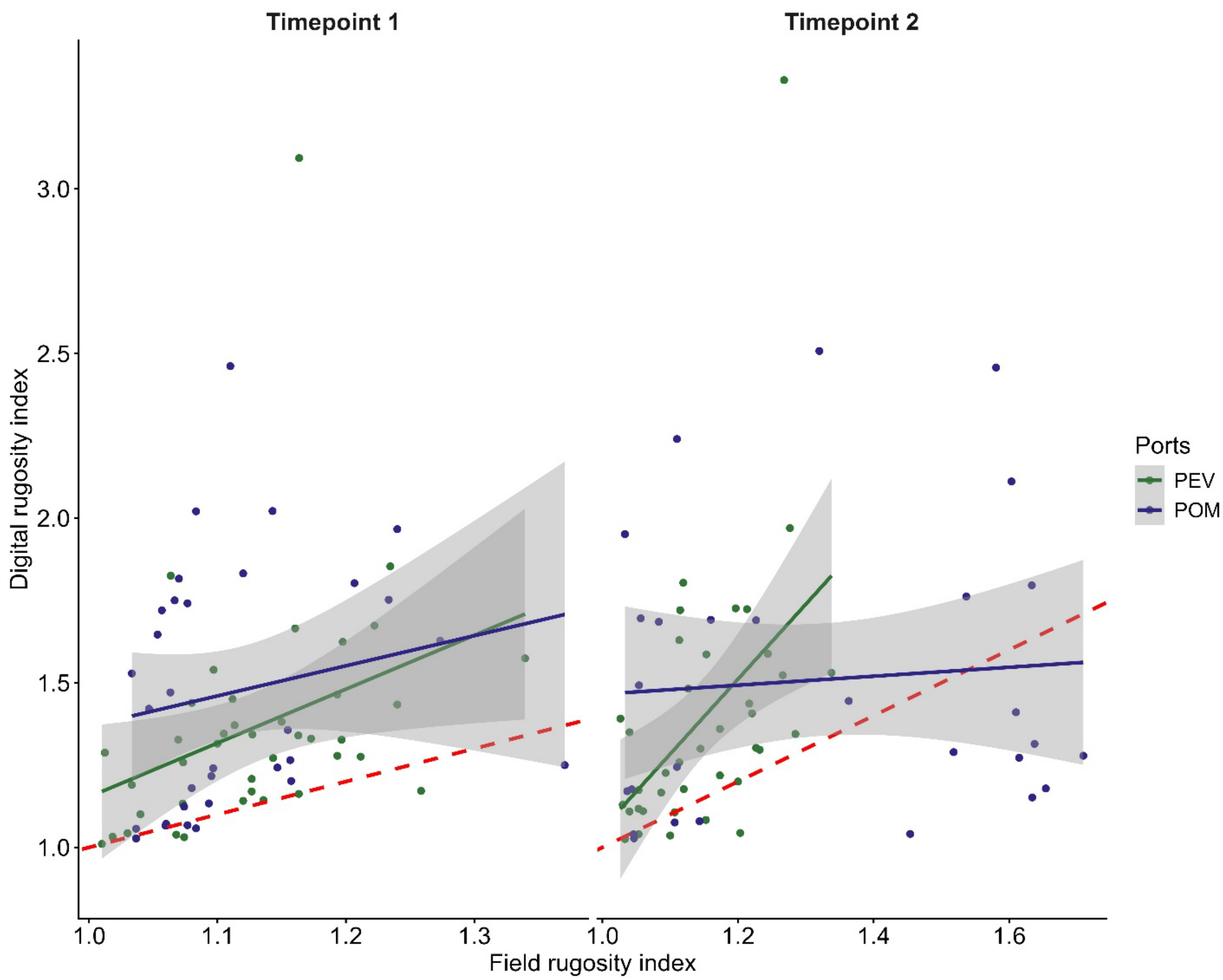

Figure 6.5.1: *Linear association between field (x-axis) and digital rugosity (y-axis) measurements at the micro-scale (within submeter quadrats) for both PEV – Port Everglades (green line) and POM – Port of Miami (dark blue line) between both time points (t1 – first time point, t2 – second time point). The red dotted line illustrates the 1:1 association between the two measurements, and the gray-shaded areas display the confidence interval around the linear model trend line.*

3.5.1.2 Log response ratio analysis to assess temporal responses between methods

Log response ratio (LRR) was used to quantify the proportional change of rugosity between the two time points. Specifically, a linear model was fitted to assess differences in the temporal rugosity response between the field and digital methods, and across reef types. The models are well-fitted; however, the field model explained more variance than the digital model (field $R^2 = 0.74$, digital $R^2 = 0.33$, ***Table 6.5.2***). The plot illustrating the LRR patterns (Figure 6.5.2) shows that the two methods agree on one broad pattern – i.e., rugosity changed more in some reef types than others, but they disagree on where. In PEV, the digital method captured a large change primarily at the Nearshore Complex reef (LRR estimate = +0.22, $p < 0.001$; Table 6.5.2; Figure 6.5.2, **left panel**). This method also captured a Nearshore Complex change in rugosity at POM, but to a lesser degree. Also, in PEV, both methods showed log ratios near zero, with method- and reef-specific associated variance. The largest response in POM was captured using the field method on the Outer reef (LRR estimate = +0.34, $p < 0.001$; Table 6.5.2; Figure 6.5.2, **right panel**). Similarly, the field method captured a positive LRR in the PEV's Outer reef; still, the POM Outer Reef response is ~3× larger. This method also demonstrated that the Nearshore Complex, Inner reef, and Middle reefs cluster near zero across both locations (i.e., insignificant changes in rugosity between t1 and t2). These results, together with the above results on the correlation estimates, demonstrate a disconnect that could have been caused by either systematic or random measurement errors, or by scale-specific rugosity patterns captured by both methods.

Table 6.5.2: *Summary of linear models assessing the temporal log response ratio (*$i.e., LRR = log\frac{rugosity_{t2}}{rugosity_{t1}}$*) of field and digital rugosity measurements at the micro-scale (within submeter quadrats). The table summarizes the LRR models that included location (PEV – Port Everglades, POM – Port of Miami) and reef type, with their interaction as a fixed factor. The summary table includes the coefficient of variation or determination (*R^2*), the F-statistic, and p-values, with the respective sample sizes for testing the difference between the models with the fixed factors and a null model (*$H0: \beta1 = \beta2 = \cdots ... = \beta k = 0$*).*

Observation Type	R^2	Adj. R^2	F-statistic	p-value	n
Field	0.740	0.708	23.265	0.000	56
Digital	0.328	0.243	3.831	0.003	54

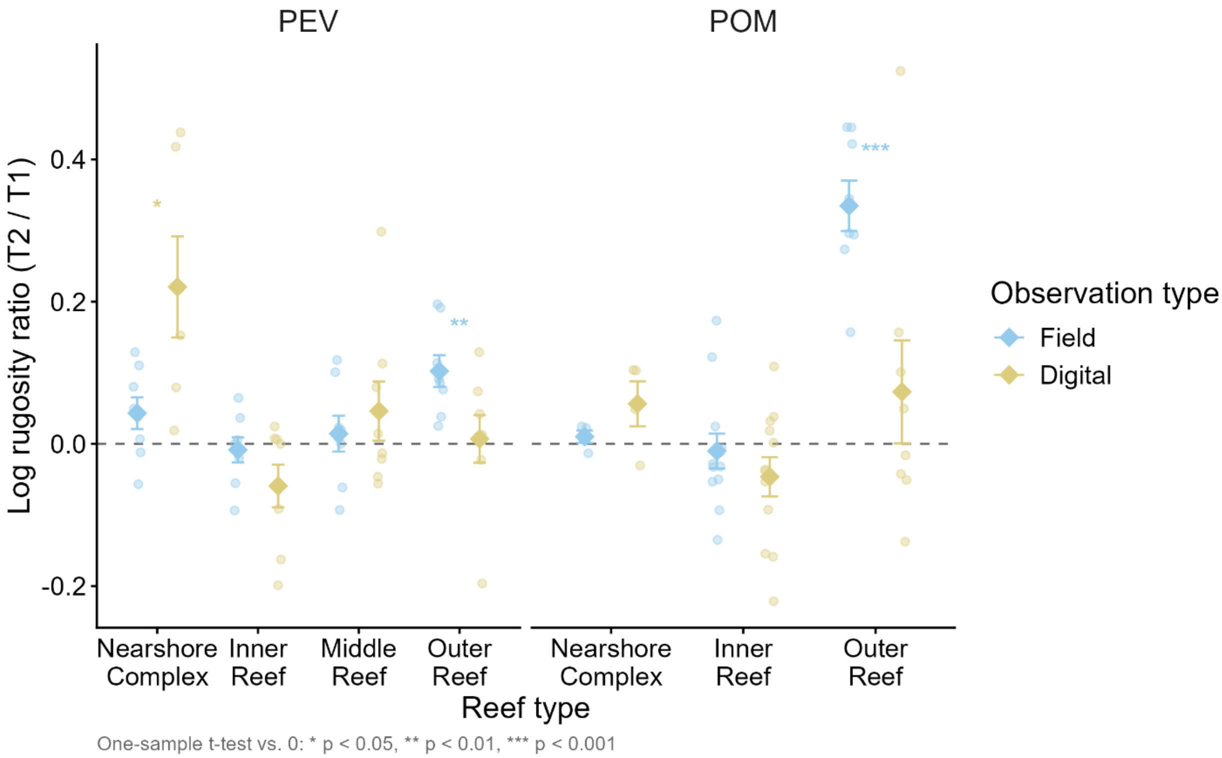

Figure 6.5.2: *Temporal log response ratio* ($i.e., LRR = log\frac{rugosity_{t2}}{rugosity_{t1}}$) *of field (light blue) and digital (gold) rugosity measurements at the micro-scale in PEV – Port Everglades (left panel) and POM – Port of Miami (right panel). The dark grey dotted line marks LRR = 0 or no difference between rugosity measurements between the first and second timepoint – i.e., Positive values indicate increased rugosity compared to timepoint 1, while negative values indicate decreased rugosity relative to timepoint 1. Asterisks denote LRR values that significantly deviated from 0.*

3.5.1.3 Analysis of variance to determine sources of divergence between methods

The overall poor agreement among methods was largely driven by POM observations, in which digital rugosity appears to reflect something other than the *in-situ* structural complexity captured by field measurements. Subsequent analyses of the variance were performed to assess potential causes of disagreement. First, the distribution of variance across locations (PEV vs POM) and methods (field vs digital) was compared to assess whether low variance could have buffered the real correlation between methods. This assessment showed that field rugosity is narrowly distributed with tightly clustered near 1.0–1.2 in all groups, while digital rugosity is right-skewed with much longer tails (**Figure 6.5.3**). Field variance at POM during the first time point is nearly equal to the variance in PEV during the same period (SD 0.078 vs. 0.075); thus, showing that compressed field measurements are not uniquely a POM problem (**Table 6.5.3**). The distributional mismatch between methods is most severe during the second time point, especially in POM (SD 0.25 vs 0.81), which corresponds exactly to the weakest correlation (r = 0.08) (**Figure 6.5.3**, **Table 6.5.3**). These discrepancies, including the bimodal distribution in the field methods (**Figure 6.5.3 Lower Right Panel**), suggest that the two methods capture structurally different value distributions. This pattern in value distribution, plus the unique variance, implies that the low correlations are not due to random noise (random or systematic measurement errors), but rather reflect the digital method resolving finer-scale structural complexity.

Table 6.5.3: *Summary of the variance of field and digital rugosity measurements at the micro-scale (within submeter quadrats) across the locations (PEV – Port Everglades, POM – Port of Miami) and time points (t1 – first time point, t2 – second time point). The summary table includes the mean and standard deviation (SD) for both methods, as well as the range of their values (Range). The table also includes the Pearson correlation coefficient between the field and digital observations - r (Field ~ Digital).*

Location	Time point	N	Mean (Field)	SD (Field)	Range (Field)	Mean (Digital)	SD (Digital)	Range (Digital)	r (Field ~ Digital)
PEV	t1	40	1.130	0.075	0.330	1.367	0.351	2.083	0.349
PEV	t2	38	1.149	0.084	0.311	1.395	0.404	2.305	0.474
POM	t1	32	1.114	0.078	0.337	1.473	0.370	1.435	0.193
POM	t2	28	1.326	0.256	0.676	1.510	0.433	1.480	0.080

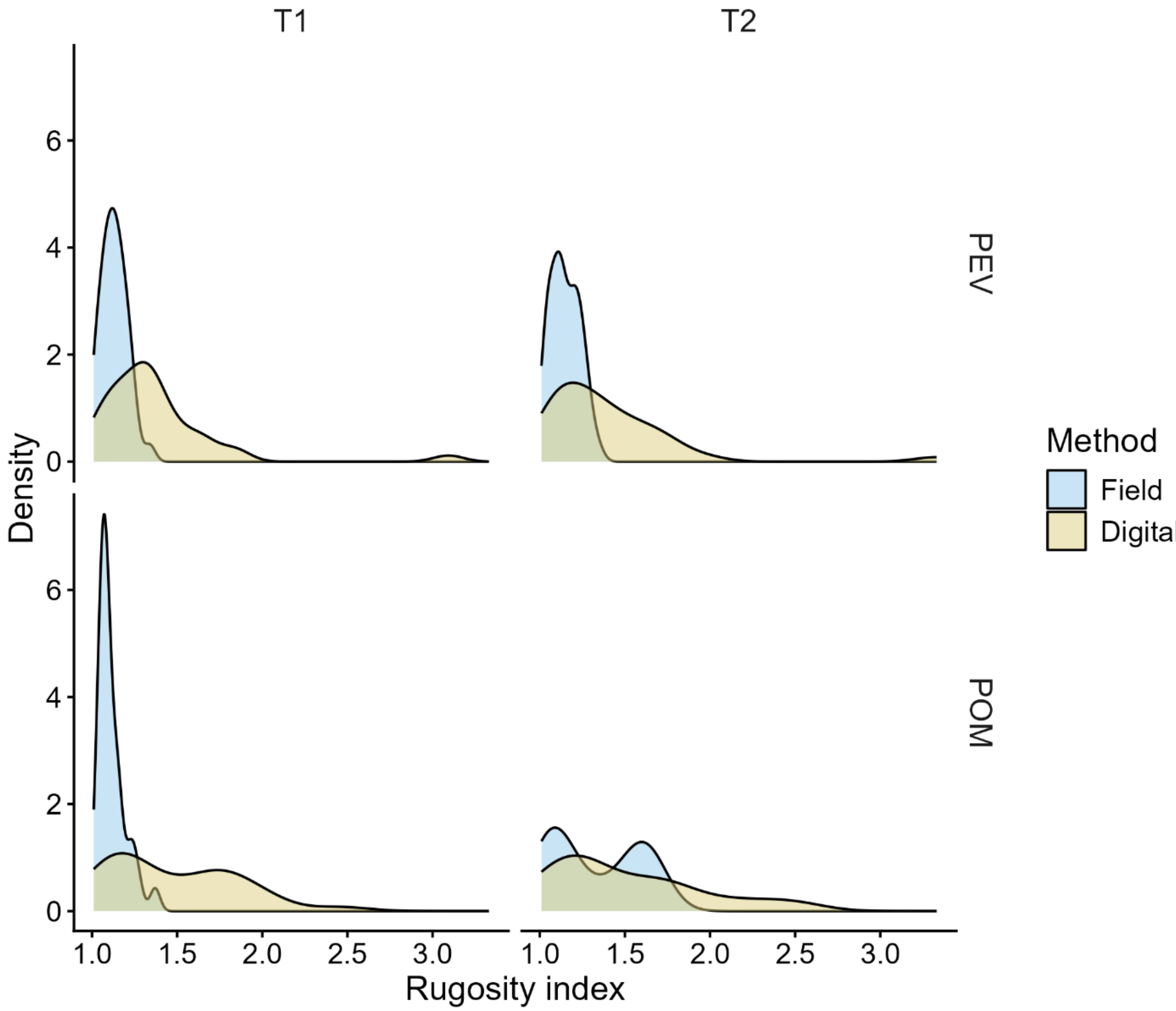

Figure 6.5.3: *Density plots showing the value distribution of rugosity measurements using field (light blue) and digital (gold) methods at the micro-scale in PEV – Port Everglades (upper panel) and POM – Port of Miami (lower panel). The vertical panels (columns) show the distribution of values between the first (left panel) and second timepoint (right panel).*

In addition to the analysis of variance above, we calculated the coefficient of variation between field and digital micro-rugosity measurements across reef types to assess whether divergence between the methods, particularly in POM, was driven by inherent reef structural characteristics (**Figure 6.5.4**). Field CV is consistently lower than digital across all reef types (CV ratio < 1 in most transects), demonstrating that field measurements are generally less variable within submeter quadrats, which is the opposite of the expected pattern if the field chain-and-tape method was more sensitive to fine reef structural characteristics. However, the CV ratio plot reveals outliers with ratios > 1 (and up to ~8) concentrated at low mean rugosity (near 1.0), primarily at PEV Inner Reef and Middle Reef types. These are the cases in which the field becomes more variable (unstable), thereby supporting the idea that unique reef structure may influence the decoupling between methods. The trend lines for PEV decline with increasing rugosity – i.e., as structural complexity increases (higher mean rugosity), the field becomes proportionally *less* imprecise relative to digital, consistent with the idea that chain-and-tape struggles most on flat, homogeneous reef surfaces. Thus, the decoupling appears to reflect a discordance in the spatial scale of structural complexity captured by each method.

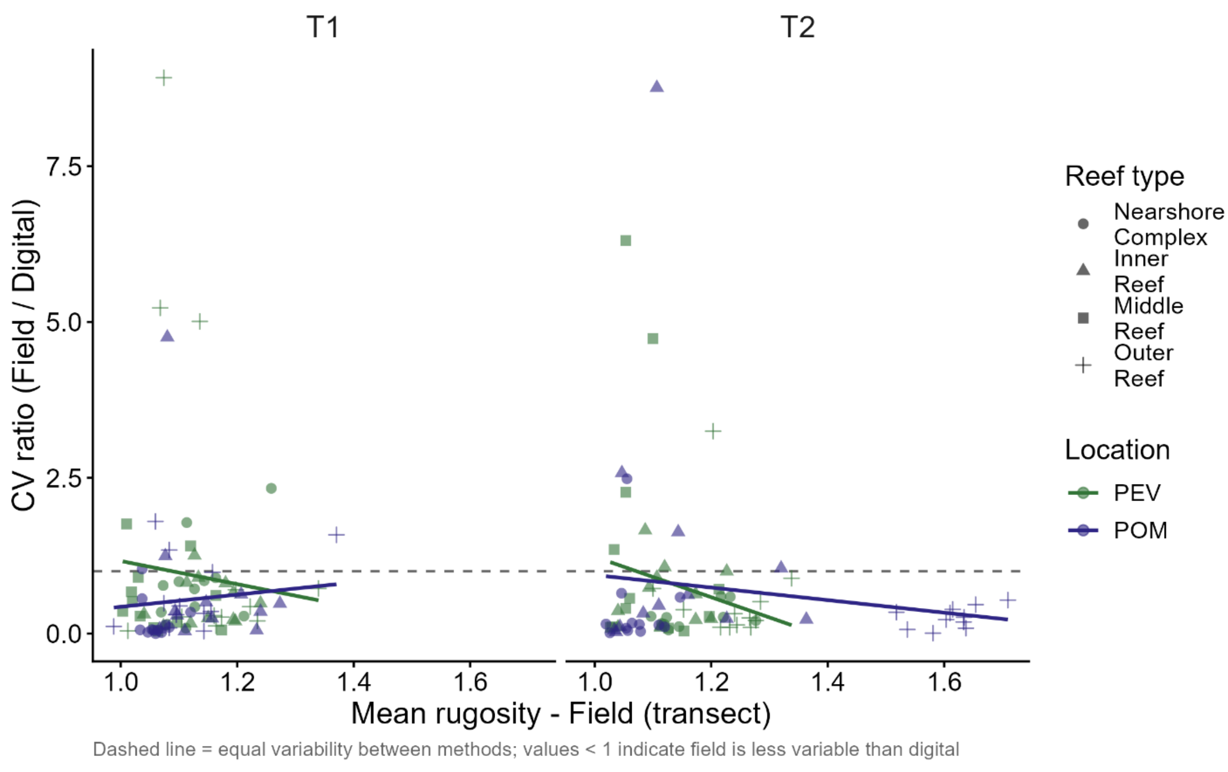

Figure 6.5.4: *Relationship between the mean rugosity values within a quadrat and the ratio of field and digital coefficient of variation measurements. A CV ratio < 1 indicates that field observations are less variable than digital observations. CV ratio – Mean Rugosity lines colored based on PEV – Port Everglades (green line) and POM – Port of Miami (dark blue line) observations between both time points (T1 – first timepoint, T2 – second timepoint).*

3.5.2 Correlation of field and digital rugosity at the macro-scale (observations over several meters)

3.5.2.1 Correlation analysis to assess the concordance

Similar to the micro-rugosity scale, the same directional pattern held at the macro scale – i.e., digital rugosity exceeded field rugosity in all groups (mean digital: 1.26–1.55; mean field: 1.09–1.14; **Table 6.5.5**, **Figure 6.5.5**). Still, the field-digital correspondence at the macro scale was similarly low. After excluding POM Plot 2 based on anomalously large and consistent residuals, R^2 values ranged from 0.05 (POM, Time point 1) to 0.19 (PEV, Time point 2), with Pearson correlations of $r = 0.08–0.43$. No regression slope deviated significantly from 1 at the macro scale, indicating similar scaling (i.e., proportional agreement) between the two methods across locations and reef types. However, this result should be interpreted with caution, considering that slope standard errors approached or exceeded the slope estimates for POM (slope coefficient $\beta = 0.47 \pm 0.46$ at T1; slope coefficient $\beta = 1.55 \pm 1.82$ at T2), suggesting that the models lacked sufficient statistical power to detect departures from a 1:1 relationship rather than to confirm proportional agreement.

Table 6.5.4: *Summary of linear models assessing the concordance between field and digital rugosity measurements at the macro-scale (across the plots). For both locations (PEV – Port Everglades, POM – Port of Miami) and time points (t1 – first time point, t2 – second time point), the table includes the coefficient of variance or determination (R^2) and slope between field and digital rugosity measurements, and the t-statistic (t (vs. 1:1)) and p-values (p (vs. 1:1)) associated with testing the difference between the observed slope and the 1:1 expected slope.*

Location	Time point	R^2	Slope	Slope SE	*t* (vs. 1:1)	*p* (vs. 1:1)
PEV	t1	0.187	0.899	0.409	-0.246	0.808
PEV	t2	0.093	0.910	0.606	-0.148	0.884
POM	t1	0.069	0.472	0.463	-1.140	0.273
POM	t2	0.053	1.546	1.815	0.301	0.768

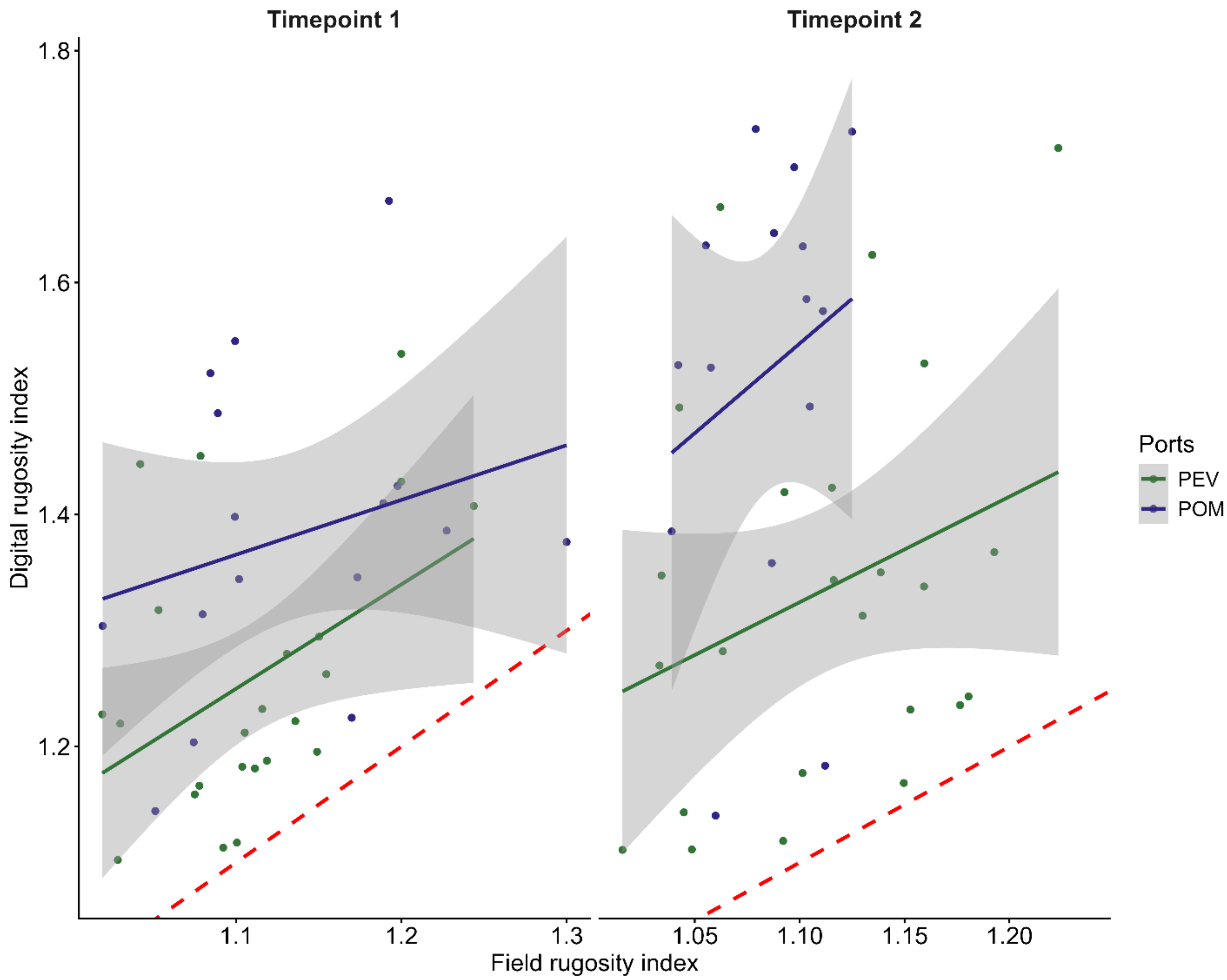

Figure 6.5.5: *Linear association between field (x-axis) and digital rugosity (y-axis) measurements at the macro-scale (across plots) for both PEV – Port Everglades (green line) and POM – Port of Miami (dark blue line) between both time points (t1 – first timepoint, t2 – second timepoint). The red dotted line illustrates the 1:1 association between the two measurements, and the gray-shaded areas display the confidence interval around the linear model trend line.*

3.5.2.2 Analysis of variance to determine sources of divergence between methods

Similar to the microscale rugosity measurements, digital rugosity exhibited a substantially greater distributional spread than field measurements at the macroscale. Field rugosity observations at the plot level were also compressed, with SD values ranging from 0.036 to 0.073 and a total range of 0.14 to 0.28, in contrast to digital observations, which ranged from 0.12 to 0.20, yielding SD ratios of 2.07–5.47 (**Table 6.6.6**). Density plots confirmed this structure (**Figure 6.6.6**) by showing that field rugosity was unimodal and tightly clustered near values of 1.0–1.3 at both scales, while digital rugosity displayed right-skewed or bimodal distributions, most notably at POM during the second time point, where a secondary mode above 1.4 was apparent in the digital density but absent in the field distribution. This decoupling of variance reinforces that the two methods are not measuring a shared underlying structural signal.

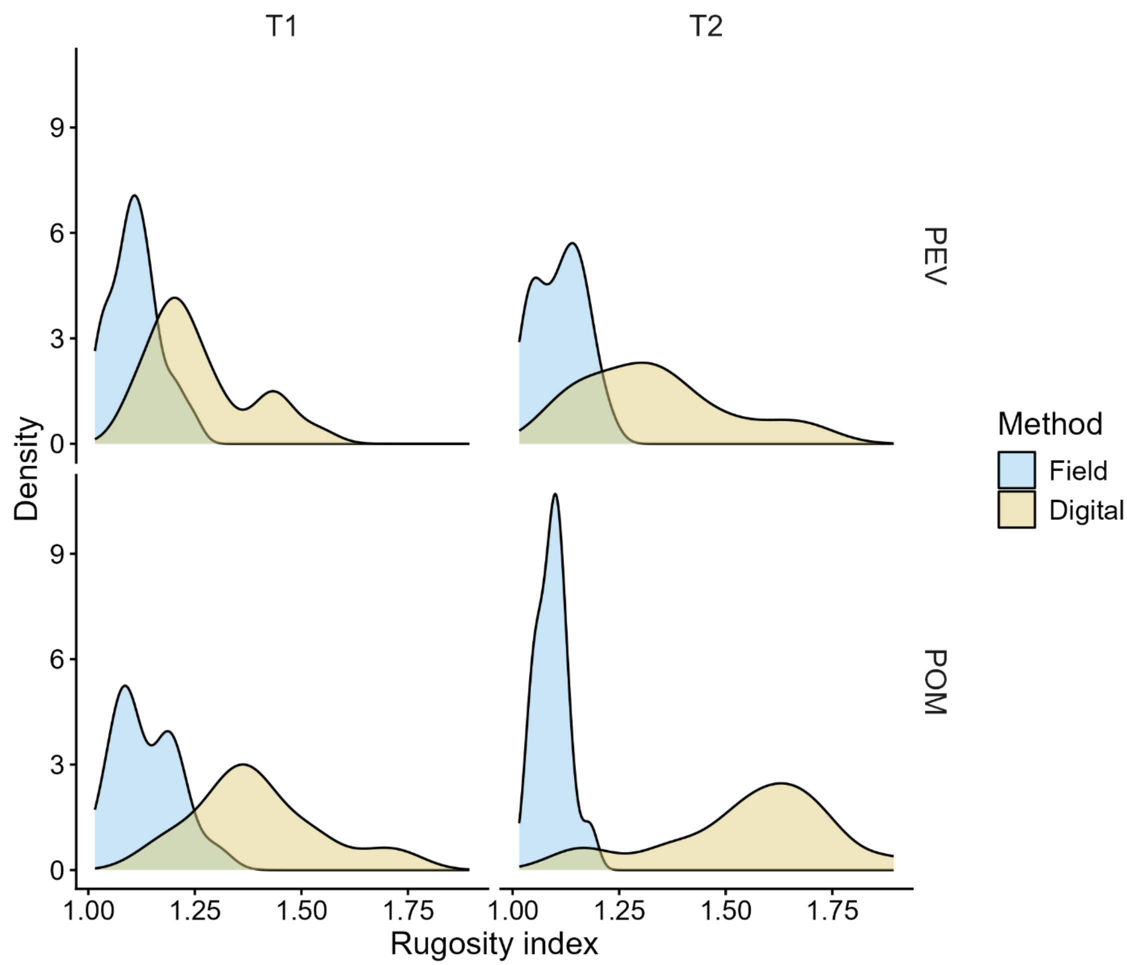

Figure 6.6.6: *Relationship between the mean rugosity values within a quadrat and the ratio of field and digital coefficient of variation measurements. A CV ratio < 1 indicates that field observations are less variable than digital observations. CV ratio – Mean Rugosity lines colored based on PEV – Port Everglades (green line) and POM – Port of Miami (dark blue line) observations between both time points (T1 – first time point, T2 – second time point).*

Table 6.5.5: *Summary of the variance of field and digital rugosity measurements at the macro-scale (across plots) across the locations (PEV – Port Everglades, POM – Port of Miami) and time points (t1 – first time point, t2 – second time point). The summary table includes the mean and standard deviation (SD) for both methods, as well as the range of their values (Range). The table also includes the Pearson correlation coefficient between the field and digital observations - r (Field ~ Digital).*

Location	Time point	N	Mean (Field)	SD (Field)	Range (Field)	Mean (Digital)	SD (Digital)	Range (Digital)	r (Field ~ Digital)
PEV	t1	23	1.109	0.058	0.225	1.258	0.120	0.436	0.432
PEV	t2	24	1.111	0.058	0.208	1.334	0.173	0.605	0.305
POM	t1	18	1.135	0.073	0.281	1.397	0.154	0.597	0.082
POM	t2	17	1.093	0.036	0.142	1.554	0.197	0.754	0.405

Rest of page intentionally left blank.

SECTION IV – KEY FINDINGS, DISCUSSION, AND MANAGEMENT RECOMMENDATIONS

This project demonstrates that Structure-from-Motion (SfM) photogrammetry, large-area images (LAIs), and 3D digital models can provide management-relevant information on sedimentation effects that is difficult to obtain using traditional field methods alone. Across reef habitats near Port Everglades (PEV) and Port of Miami (POM), these tools captured spatial patterns in sediment cover, benthic composition, colony-level responses, and reef structural complexity at resolutions that are directly useful for coral reef monitoring and adaptive management near ports and other sediment-generating activities. However, interpretations should be framed within the spatial and temporal limitations of the study design, including the short interval between sampling periods and the relatively small number of sites per habitat type, limitations currently being addressed by phase II of this project. Below, we synthesize the main findings, especially in the context of coral reef monitoring and the project's goals.

Key finding 1. Sediment-dominated habitats were common, but sediment exposure varied strongly among reef types

Across all surveyed habitats, unconsolidated sediment (sand) represented the dominant benthic component, while hard coral cover remained uniformly low. The most pronounced spatial pattern was observed at the PEV Middle Reef, where sand cover was substantially higher than in other reef zones and sponge cover was comparatively reduced. These findings are consistent with the interpretation that sediment exposure varies among reef types and may be influenced by geomorphology and proximity to sand channels. From a management perspective, these results suggest that sedimentation pressure is likely spatially heterogeneous and that reef geomorphology and geographic context may be important factors controlling exposure to sediment accumulation.

Key finding 2. Limited short-term temporal change, with detectable shifts in sediment cover

As expected, considering the short timeframe, temporal differences in benthic cover between the two sampling periods (~2–3 months apart) were generally small and not statistically significant for most functional groups. However, via LAIs, a significant increase in sand cover at POM during the second sampling period was detected. While the study's short duration limits interpretation of seasonal trends, this result demonstrates that LAI-based measurements can detect relatively small changes in unconsolidated sediment cover over short time frames. These findings should be interpreted cautiously, as longer time series are required to evaluate seasonal or event-driven sediment dynamics.

Key finding 3. Digital image-based assessments can reliably capture broad sediment-stress patterns

Comparisons between field observations and digital image classifications showed strong agreement for sponge sediment-stress indicators, with 73.2% overall agreement and especially strong correspondence for the sediment accumulation category. This indicates that LAI-based assessments can reliably detect broad sediment-associated condition classes and can reproduce much of the information typically collected through diver observations.

Key finding 4. Coral colony size change signals are detectable but require cautious interpretation

Analyses of colony size change indicated that coral colonies at PEV exhibited a lower probability of growing than at POM and reduced growth in inner reef habitats relative to Nearshore Complex reefs. Additional log response ratio analyses based on size differences between the time points suggested negative or near-zero growth in several reef zones, particularly at the PEV Middle Reef. Given the short sampling interval and the slow growth rates of most coral species, these patterns should be interpreted as preliminary indicators rather than definitive evidence of sediment-driven growth responses. However, the ability to quantify colony-size changes from orthoprojected LAIs represents a methodological advancement that may improve the detection of subtle changes (e.g., partial mortality or shrinkage) in future longer-term studies.

Key finding 5. Feasibility of using 3D models to quantify fine-scale structural variation

SfM-derived 3D models successfully generated digital rugosity metrics at both micro- and macro-scales. However, correspondence between field (chain-and-tape) and digital rugosity measurements was generally weak, particularly at POM. Overall, the results showed that the field method produces systematically narrow, unimodal distributions of rugosity values regardless of reef type or spatial scale, whereas digital photogrammetry discriminates more finely among reef types and resolves greater within-transect heterogeneity (i.e., digital metrics resolved finer-scale heterogeneity than field measurements). These findings suggest that field and digital methods quantify different aspects of reef structural complexity and should not be treated as interchangeable metrics.

Key finding 6. Grain-size composition shifts toward finer sediment over time, with the strongest changes at PEV

Sediment grain-size composition was dominated by coarse sand (250–500 μm) across all reef zones and both locations, but both Port Everglades (PEV) and Port of Miami (POM) showed a compositional shift toward finer grain sizes between timepoints. The 35–53 μm fraction increased, with PEV showing a particularly pronounced increase, roughly tripling in raw proportional terms compared to POM. The most statistically robust signal of divergence between locations was a significant location × timepoint interaction in the 125–250 μm fraction ($p = 0.017$): the two ports did not differ in this size class at T1, but by T2 PEV had substantially less mid-sized sediment than POM, indicating the locations are diverging compositionally over time. Notably, PEV accumulated 18% more total sediment mass by T2 compared to only 4% at POM, consistent with net sediment addition potentially linked to the Port Everglades sand bypass project. Middle and Outer reef zones exhibited disproportionately high fine sediments relative to Nearshore Complex and Inner Reef zones at both locations, reflecting the role of wave energy and hydrodynamic sorting in structuring grain-size gradients across the reef profile.

Key finding 7. Implications for monitoring approaches

Collectively, the results indicate that SfM photogrammetry and LAIs provide a scalable and repeatable approach for quantifying multiple components of reef condition, including sediment cover, benthic composition, selected biological responses, and structural complexity. At the same time, limitations related to temporal coverage, habitat replication, and method-specific sensitivities should be considered when interpreting results or integrating these tools into regulatory frameworks. Still, based on the study findings, SfM photogrammetry and LAIs are most useful for supporting habitat-specific sediment monitoring by identifying reef zones with persistent or elevated sediment accumulation, as well as for baseline and compliance monitoring by enabling the detection of changes before, during, and after dredging or other coastal construction activities. In addition, these approaches provide valuable archival documentation through permanent, spatially explicit records that can be revisited for longitudinal and time-series analyses, and they facilitate integrated assessments by linking sediment exposure with benthic community composition and fine-scale structural metrics within a single, cohesive analytical framework.

Rest of page intentionally left blank.

SECTION V – REFERENCES

Carvalho, R. C., & Reef, R. (2022). Quantification of Coastal Change and Preliminary Sediment Budget Calculation Using SfM Photogrammetry and Archival Aerial Imagery. *Geosciences*, *12*(10), 357. https://doi.org/10.3390/geosciences12100357

Couch, Courtney et al. (2021). Comparing coral demographic surveys from in situ observations and Structure-from-Motion imagery shows low methodological bias. https://doi.org/10.25923/307k-fk90

David, C. G., Kohl, N., Casella, E., Rovere, A., Ballesteros, P., & Schlurmann, T. (2021). Structure-from-Motion on shallow reefs and beaches: Potential and limitations of consumer-grade drones to reconstruct topography and bathymetry. *Coral Reefs*, *40*(3), 835–851. https://doi.org/10.1007/s00338-021-02088-9

Dietrich, J. T. (2016). Riverscape mapping with helicopter-based Structure-from-Motion photogrammetry. *The Natural and Human Structuring of Rivers and Other Geomorphic Systems: A Special Issue in Honor of William L. Graf*, *252*, 144–157. https://doi.org/10.1016/j.geomorph.2015.05.008

Edwards, C. B., Eynaud, Y., Williams, G. J., Pedersen, N. E., Zgliczynski, B. J., Gleason, A. C. R., Smith, J. E., & Sandin, S. A. (2017). Large-area imaging reveals biologically driven non-random spatial patterns of corals at a remote reef. *Coral Reefs*, *36*(4), 1291–1305. https://doi.org/10.1007/s00338-017-1624-3

Ferrari, R., Bryson, M., Bridge, T., Hustache, J., Williams, S. B., Byrne, M., & Figueira, W. (2016). Quantifying the response of structural complexity and community composition to environmental change in marine communities. *Global Change Biology*, *22*(5), 1965–1975. https://doi.org/10.1111/gcb.13197

Fukunaga, A., Burns, J. H. R., Craig, B. K., & Kosaki, R. K. (2019). Integrating Three-Dimensional Benthic Habitat Characterization Techniques into Ecological Monitoring of Coral Reefs. *Journal of Marine Science and Engineering*, *7*(2), 27. https://doi.org/10.3390/jmse7020027

Guzman, S., Ladd, M. C., Rodriguez-Ruano, V., Barriera, W., Velazquez, J., & Duran, A. (2026). The abundance, formation, and persistence of long sediment-laden algal turfs on Florida's coral reef. *Frontiers in Marine Science*, *13*, 1792492. https://doi.org/10.3389/fmars.2026.1792492

Rivas, N., James, W. R., Bautista, V., Sandquist, M., Guerriero, A. F., Arias, S. B., Mercado-Molina, A. E., Rehage, J., & Santos, R. O. (2026). Tipping the balance: Reef community shifts after a regional urchin population collapse. *Coral Reefs*. https://doi.org/10.1007/s00338-026-02822-1

Royer, J.-P., Nawaf, M., Merad, D., Saccone, M., Bianchimani, O., Garrabou, J., Ledoux, J.-B., Lopez-Sanz, A., & Drap, P. (2018). Photogrammetric Surveys and Geometric Processes to Analyse and Monitor Red Coral Colonies. *Journal of Marine Science and Engineering*, *6*(2), 42. https://doi.org/10.3390/jmse6020042

Serrano, X. M., Chacin, D. H., Mack, K., Gregg, K., Parsons, M., Ladd, M., Lehmann, W., Wolfe, J., & Karazsia, J. (2026). A rapid method to assess sediment deposition and stress on coral reef benthic taxa resulting from dredging and other sediment disturbances. *Marine Pollution Bulletin*, *222*, 118629. https://doi.org/10.1016/j.marpolbul.2025.118629

Simmons, K. R., Bohnenstiehl, D. R., & Eggleston, D. B. (2022). Spatiotemporal Variation in Coral Assemblages and Reef Habitat Complexity among Shallow Fore-Reef Sites in the Florida Keys National Marine Sanctuary. *Diversity*, *14*(3), 153. https://doi.org/10.3390/d14030153

Spyksma, A. J. P., Miller, K. I., & Shears, N. T. (2022). Diver-generated photomosaics as a tool for monitoring temperate rocky reef ecosystems. *Frontiers in Marine Science*, *9*, 953191. https://doi.org/10.3389/fmars.2022.953191

Stojic, M., Chandler, J., Ashmore, P., & Luce, J. (1998). The Assessment of Sediment Transport Rates by Automated Digital Photogrammetry. *Photogrammetric Engineering & Remote Sensing*, *64*(5), 387–395.

Walker, B. K., Gilliam, D. S., Dodge, R. E., & Walczak, J. (2012). *Dredging and Shipping Impacts on Southeast Florida Coral Reefs*.

Wu, M.-H. M., Ribas-Deulofeu, L., Liu, C.-H. E., Nozawa, Y., & Denis, V. (2025). Benthic drivers of structural complexity in coral reefs across a tropical-subtropical transition zone. *Frontiers in Marine Science*, *12*, 1513498. https://doi.org/10.3389/fmars.2025.1513498